Cyclic nucleotide-induced bidirectional long-term synaptic plasticity in *Drosophila* mushroom body

Daichi Yamada[1] and Toshihide Hige*[1,2,3]

[1]Department of Biology, University of North Carolina at Chapel Hill, Chapel Hill, United States

[2]Department of Cell Biology and Physiology, University of North Carolina at Chapel Hill, Chapel Hill, United States

[3]Integrative Program for Biological and Genome Sciences, University of North Carolina at Chapel Hill, Chapel Hill, United States

***Correspondence:**
Toshihide Hige
hige@email.unc.edu

Abstract

Activation of the cyclic adenosine monophosphate (cAMP) pathway generally facilitates synaptic transmission, serving as one of the common mechanisms underlying long-term potentiation (LTP). In the *Drosophila* mushroom body, simultaneous activation of odor-coding Kenyon cells (KCs) and reinforcement-coding dopaminergic neurons synergistically activates adenylyl cyclase in KC presynaptic terminals, which is believed to trigger synaptic plasticity underlying olfactory associative learning. However, learning induces long-term depression (LTD) at these synapses, contradicting the universal role of cAMP as a facilitator of transmission. Here, we develop a system to electrophysiologically monitor both short-term and long-term synaptic plasticity of KC output synapses and demonstrate that *Drosophila* mushroom body is indeed a rare, if not the only, exception where increase in cAMP level induces LTD. In contrary to the prevailing model, we find that cAMP increase alone is insufficient for plasticity induction; it additionally requires KC activation to replicate presynaptic LTD induced by pairing of dopamine and KC activation. On the other hand, activation of the cyclic guanosine

26 monophosphate pathway paired with KC activation induces slowly developing LTP, proving
27 antagonistic actions of the two second-messenger pathways predicted by behavioral study.
28 Furthermore, subtype-specific interrogation of KC output synapses reveals that different KC
29 subtypes exhibit distinct plasticity duration even among synapses on the same postsynaptic
30 neuron. Thus, our work not only revises the role of cAMP in synaptic plasticity by uncovering
31 unexpected convergence point of the cAMP pathway and neuronal activity, but also establishes
32 the methods to address physiological mechanisms of synaptic plasticity in this historically
33 important model system.

34 **Introduction**

35 Synaptic plasticity is a fundamental mechanism of learning. *Aplysia*, the same animal that helped
36 prove this notion for the first time, also contributed to the identification of cyclic adenosine
37 monophosphate (cAMP)-dependent pathway as a key molecular basis for synaptic plasticity
38 (Brunelli *et al.*, 1976; Castellucci *et al.*, 1980). Following this discovery, the cAMP/protein
39 kinase A (PKA) pathway was found to be one of the ubiquitously important mechanisms
40 underlying learning-related synaptic plasticity in both vertebrates and invertebrates (Kandel *et*
41 *al.*, 2014). In agreement with other systems, behavioral genetics studies in *Drosophila* have
42 linked learning defects in olfactory classical conditioning to mutations of the cAMP/PKA
43 pathway genes, such as cAMP phosphodiesterase *dunce* (Byers *et al.*, 1981) and
44 calcium/calmodulin-activated adenylyl cyclase (AC) *rutabaga* (Livingstone *et al.*, 1984).

45 The mushroom body (MB) is the central brain area for olfactory learning in *Drosophila*. A given
46 odor evokes reliable spiking responses in a sparse population (~5%) of the ~2,000 Kenyon cells
47 (KCs), the principal neurons of the MB (Turner *et al.*, 2008; Honegger *et al.*, 2011). KCs form
48 dense axon bundles, constituting the MB lobes, where they synapse on their main postsynaptic
49 partners, MB output neurons (MBONs). In the MB lobes, KCs also receive dense inputs from the
50 dopaminergic neurons (DANs), which, depending on cell types, convey either reward or
51 punishment signals during conditioning (Schwaerzel *et al.*, 2003; Liu *et al.*, 2012; Burke *et al.*,
52 2012; Aso & Rubin, 2016). Thus, olfactory and reinforcement signals converge at the KC axons.
53 This notion is consistent with the fact that memory defects of the mutants of a G_s-linked

54 dopamine receptor *Dop1R1* (Kim *et al.*, 2007; Qin *et al.*, 2012) and *rutabaga* (McGuire *et al.*,
55 2003; Blum *et al.*, 2009) can be fully rescued by expressing the corresponding functional
56 proteins in KCs. These results led to the prevailing working model that Rutabaga AC in the KC
57 axons acts as a coincidence detector of olfactory and reinforcement signals, represented by
58 calcium influx and dopamine input, respectively, and the resulting increase in cAMP level
59 induces presynaptic plasticity at KC-MBON synapses (Heisenberg, 2003). In support of this
60 model, coactivation of KCs and dopamine receptors synergistically activates cAMP/PKA
61 pathway in KC axons (Tomchik & Davis, 2009; Gervasi *et al.*, 2010; Handler *et al.*, 2019; but
62 see also Abe *et al.*, 2023).

63 In general, action of cAMP on synaptic transmission is excitatory. cAMP increase virtually
64 always results in potentiation of synapses in both vertebrates and invertebrates. The examples
65 range from synaptic facilitation of the siphon sensory neurons in *Aplysia* (Goldsmith & Abrams,
66 1991) to long-term potentiation (LTP) in rodent hippocampus (Huang *et al.*, 1994) and
67 cerebellum (Salin *et al.*, 1996). Conversely, decrease in cAMP underlies multiple forms of long-
68 term depression (LTD) (Tzounopoulos *et al.*, 1998; Chevaleyre *et al.*, 2007). This positive
69 relationship between cAMP level and synaptic strength also seems to apply to *Drosophila* as
70 elevated presynaptic cAMP level mediates post-tetanic synaptic potentiation at the
71 neuromuscular junction (Kuromi & Kidokoro, 2000), which was impaired in *dunce* and *rutabaga*
72 mutants (Zhong & Wu, 1991). Furthermore, multiple pioneering studies of either early (Wang *et*
73 *al.*, 2008) or late phase (Yu *et al.*, 2006; Akalal *et al.*, 2010) of memory traces induced by
74 olfactory learning reported potentiation of odor-evoked calcium activity in the KC axons. Given
75 this historic background, it was rather unexpected that pairing of odor presentation and
76 optogenetic activation of DANs induces robust LTD at KC-to-MBON synapses (Hige *et al.*,
77 2015). However, LTD but not LTP fits the circuit logic of the MB. Anatomically, a given cell
78 type of MBONs has partner cell types of DANs, and they show matching innervation patterns in
79 the MB lobes (Aso *et al.*, 2014*b*). In general, activation of MBONs signals the valence that is
80 opposite to the one signaled by the partner DANs (Aso *et al.*, 2014*a*; Owald *et al.*, 2015; Aso &
81 Rubin, 2016). Thus, punishment-encoding DANs can induce LTD in approach-directing MBONs
82 during aversive learning. Although numerous other studies now support or confirm that odor-
83 specific depression in MBON responses underlies olfactory learning (Séjourné *et al.*, 2011;
84 Owald *et al.*, 2015; Cohn *et al.*, 2015; Perisse *et al.*, 2016; Berry *et al.*, 2018; Felsenberg *et al.*,

85 2018; Handler *et al.*, 2019; Awata *et al.*, 2019; Zhang *et al.*, 2019; McCurdy *et al.*, 2021;
86 Hancock *et al.*, 2022; Schnitzer *et al.*, 2022; Noyes & Davis, 2023; Zeng *et al.*, 2023), there has
87 been no direct evidence that *Drosophila* MB is an exception where cAMP-induced synaptic
88 plasticity is depression rather than potentiation. Providing such evidence is the main objective of
89 this study.

90 cAMP signaling is not the only second messenger system implicated in learning-related plasticity
91 in the *Drosophila* MB. A subset of the MB-projecting DANs releases nitric oxide (NO) as a
92 cotransmitter (Aso *et al.*, 2019). Behavioral evidence suggests that NO acts on KC axons to
93 induce plasticity that is antagonistic to dopamine-induced LTD via activation of soluble guanylyl
94 cyclase (sGC) (Aso *et al.*, 2019), although there has been no physiological evidence for it.
95 Unlike cAMP, the sign of synaptic plasticity induced by cyclic guanosine monophosphate
96 (cGMP) varies among systems and studies. While cGMP increase predominantly induces
97 presynaptic LTP in the hippocampus (Arancio *et al.*, 1995) and hyperexcitability of sensory
98 neurons in *Aplysia* (Lewin & Walters, 1999), it also induces LTD in the hippocampus (Reyes-
99 Harde *et al.*, 1999), cerebellum (Shibuki & Okada, 1991; Lev-Ram *et al.*, 1997) and
100 corticostriatal synapses (Calabresi *et al.*, 1999). At *Drosophila* neuromuscular junction, cGMP
101 exerts an excitatory (Wildemann & Bicker, 1999) or no effect (Caplan *et al.*, 2013). Furthermore,
102 NO-dependent modulation of the *Drosophila* neuromuscular junction also involves cGMP-
103 independent, S-nitrosylation of proteins (Robinson *et al.*, 2018). Thus, it is important to
104 determine the role of cGMP in KC-to-MBON synaptic plasticity.

105 In this study, we developed an *ex vivo* system to test physiological and pharmacological
106 properties of the synaptic plasticity at KC-to-MBON synapses. In this system, we made whole-
107 cell recordings from a target MBON to monitor the excitatory postsynaptic currents (EPSCs)
108 evoked by optogenetic stimulation of a small subset of KCs, while focally injecting various
109 reagents to the MB lobe at the dendritic region of the MBON to induce or inhibit long-term
110 plasticity. This system also allowed us to monitor short-term synaptic plasticity by delivering
111 paired-pulse stimulation to test the involvement of presynaptic factors in synaptic changes
112 (Zucker & Regehr, 2002). We show that pairing of KC activation and dopamine injection induces
113 LTD accompanied by an increase in paired-pulse ratio (PPR). Unexpectedly, however, activation
114 of AC by forskolin alone was insufficient to induce qualitatively similar LTD; it required

115 simultaneous KC activation in addition to forskolin application. Pairing of pharmacological
116 activation of sGC and KC activation induced LTP accompanied by a decrease in PPR. Our
117 system also allowed for subtype-specific activation of KCs that synapse on the same MBON and
118 revealed distinct durations of synaptic plasticity between different KC subtypes. Thus, our work
119 not only revises the role of cAMP in synaptic plasticity by revealing unexpected convergence
120 point of the cAMP pathway and neuronal activity, but also establishes the methods to address
121 physiological mechanisms of synaptic plasticity.

122 **Results**

123 **Optogenetic paired-pulse stimulation of KCs can be used to assess presynaptic changes in**
124 **synaptic transmission**

125 In the field of synaptic physiology, paired-pulse protocol is commonly used to assess the
126 presynaptic strength of synaptic transmission because the paired pulse ratio (PPR), calculated as
127 the second EPSC amplitude divided by the first one, generally inversely correlates with
128 presynaptic vesicular release probability (Zucker & Regehr, 2002). Although paired EPSCs are
129 typically evoked by fiber stimulation using extracellular electrodes, similar inference can be
130 made using optogenetically delivered paired pulses (Britt *et al.*, 2012; Creed *et al.*, 2016; Liu *et*
131 *al.*, 2020). This approach is applicable to *Drosophila* KCs whose densely packed, small bundle
132 of axons deters the use of an electrode. Since this method has never been used in the *Drosophila*
133 MB, to our knowledge, we first asked whether release probability change can induce predicted
134 change in the PPR.

135 Among dozens of MBONs, we targeted MBON-γ1pedc because the relatively thick and short
136 primary neurite of this neuron allows for superior membrane voltage control (i.e. space clamp)
137 during somatic voltage-clamp recordings and also because the LTD has been best characterized
138 in this MBON using pairing of odor and DAN activation (Hige *et al.*, 2015). MBON-γ1pedc
139 receives the majority of its inputs from the γ subtype of KCs as well as a minor fraction from α/β
140 KCs in the pedunculus region of the MB (Fig. 1A). We therefore first focused on γ KC-to-
141 MBON-γ1pedc synaptic transmission. To selectively study these synapses, we expressed red-

142 shifted channelrhodopsin, CsChrimson (Klapoetke *et al.*, 2014), in a small subset of γ KCs using
143 γ KC-specific split-GAL4 driver MB623C (Shuai *et al.*, 2023) together with a stochastic
144 expression system SPARC (Isaacman-Beck *et al.*, 2020). By using the "S" (or sparse) variant of
145 the SPARC system, we can reliably label a random ~3-7% of γ KCs (Isaacman-Beck *et al.*,
146 2020), roughly equivalent to the fraction of KCs reliably responsive to a typical odor (Honegger
147 *et al.*, 2011).

148 We made whole-cell voltage-clamp recordings from MBON-γ1pedc and delivered two 1-ms light
149 pulses 400 ms apart to measure PPRs. To test the effect of release probability decrease on PPR,
150 we changed the extracellular calcium/magnesium concentrations from 1.5/4 to 0.7/5.5 mM. This
151 manipulation decreased the first EPSC amplitude while concurrently increasing the PPR (Fig.
152 1B). Conversely, increasing the release probability by changing calcium/magnesium
153 concentrations to 5/0.5 mM facilitated the first EPSC while decreasing the PPR (Fig. 1C). Thus,
154 artificial manipulation of release probability shifted PPR in the expected manner. To test whether
155 the change in PPR is attributable to presynaptic factors, we next bath-applied a low concentration
156 of mecamylamine (10 μM), a non-competitive antagonist of the nicotinic acetylcholine receptors,
157 to reduce the availability of postsynaptic ionotropic receptors without changing the release
158 probability. This manipulation attenuated the first EPSC to an equivalent level to the low calcium
159 condition (Fig. 1D). However, this decrease was not accompanied by a change in PPR. These
160 results indicate that PPRs measured by optogenetically evoked EPSCs at KC-to-MBON synapses
161 can be used as an indicator of presynaptic modulation of transmission.

162 **Pairing γ KC activation with focal dopamine application induces presynaptic LTD**

163 Using this experimental setup, we first examined whether dopamine can induce synaptic
164 plasticity at γ KC-to-MBON-γ1pedc synapses. Previous studies that demonstrated odor-specific
165 depression in MBON responses used either actual reinforcement or direct DAN activation using
166 opto- or chemogenetics, which can promote release of not only dopamine but also cotransmitters
167 or other neuromodulators (Séjourné *et al.*, 2011; Owald *et al.*, 2015; Hige *et al.*, 2015; Cohn *et*
168 *al.*, 2015; Perisse *et al.*, 2016; Berry *et al.*, 2018; Felsenberg *et al.*, 2018; Handler *et al.*, 2019;
169 Awata *et al.*, 2019; Zhang *et al.*, 2019; McCurdy *et al.*, 2021; Hancock *et al.*, 2022; Schnitzer *et*
170 *al.*, 2022; Noyes & Davis, 2023; Zeng *et al.*, 2023). We therefore do not know whether

171 dopamine alone is sufficient for the DAN activation-induced LTD. To directly test this
172 possibility, we focally applied dopamine (1 mM) into γ1pedc subregion of the MB lobe, where
173 the dendrites of MBON-γ1pedc are located, by pressure injection via a pipette placed in the MB
174 lobe (Fig. 2A). By monitoring the signal of Texas Red-conjugated dextran infused in the pipette,
175 we confirmed that our 1-min injection protocol (30 cycles of 1-s on and 1-s off) is enough to
176 diffuse the injected solution across the entire γ1pedc, but it was largely confined to half the
177 length of the medial MB lobes (Fig. 2B). Importantly, the signal was quickly washed out before
178 resuming EPSC recording 2.5 min after the end of injection. After we paired optogenetic
179 activation of γ KCs with dopamine application for 1 min, the synapses underwent LTD, which
180 lasted at least for 17 min (Figs. 2C and 2D). In 2 of the 6 recordings, we were able to continue
181 the recording for more than 30 min after pairing. In both these cases, the LTD persisted until the
182 end of recording without any sign of recovery (data not shown). This LTD was accompanied by
183 PPR increase, which persisted for the duration of LTD (Figs. 2C and 2D). In contrast, dopamine
184 application (Figs. 2E and 2F) or γ KC activation alone (Figs. 2G and 2H) induced no change in
185 EPSC amplitude or PPR. These results indicate that coincidence of γ KC activation and
186 dopamine input can induce presynaptic LTD. To test if the action of dopamine is mediated by G_s-
187 coupled D_1-like dopamine receptors, we bath-applied a selective antagonist SCH 23390 (100
188 μM). Although application of SCH 23390 by itself had no effect on the EPSC amplitude or PPR,
189 it abolished the effect of γ KC-dopamine pairing (Figs. 2I and 2J). In contrast, bath application of
190 the solvent dimethyl sulfoxide (DMSO, 0.1%) did not have such effects, as γ KC-dopamine
191 pairing still induced robust LTD and PPR increase (Figs. 2K and 2L). Taken together, these
192 results indicate that the role of DAN activation in LTD induction described in previous studies
193 (Hige *et al.*, 2015; Cohn *et al.*, 2015; Berry *et al.*, 2018; Handler *et al.*, 2019) is attributable to
194 dopamine's action on D_1-like dopamine receptors in these synapses.

195 **Presynaptic LTD induction requires both AC activation and KC activity**

196 The dominant hypothesis in the field is that coincidence of KC activity and dopamine input
197 activates AC in KC axons to elevate cAMP concentration which in turn induces synaptic
198 plasticity. This model assumes that cAMP increase is sufficient for plasticity induction. To test
199 this long-standing but unproved hypothesis, we pharmacologically activated the AC by focally

200 injecting forskolin (20 μM) into γ1pedc region (Fig 3) as we did for dopamine. This
201 concentration of forskolin is more than enough to fully activate cAMP/PKA pathway in KCs
202 (Gervasi *et al.*, 2010). However, 1-min injection of forskolin affected neither the EPSC
203 amplitude nor PPR (Figs. 3B and 3C). Increasing the concentration of forskolin to 100 μM did
204 induce a sustained decrease in the EPSC amplitude (Figs. 3D and 3E). However, this effect did
205 not accompany a change in PPR, suggesting postsynaptic origin of the plasticity. It is possible
206 that excessive concentration of forskolin recruited AC in the MBON. In support of this idea, cell-
207 type-specific transcriptome data (Aso *et al.*, 2019) suggests that expression level of AC is much
208 higher in KCs compared to the MBON (Fig. S1). Although the lack of change in PPR does not
209 formally exclude the possibility that high concentrations of forskolin induces plasticity through
210 presynaptic mechanisms, we can at least conclude that the observed plasticity is qualitatively
211 distinct from the plasticity induced by γ KC-dopamine pairing. In other words, elevation of
212 cAMP caused by AC activation is not sufficient to replicate the dopamine-induced LTD.

213 These unexpected results prompted us to test whether KC activation in addition to cAMP
214 elevation is necessary to induce presynaptic LTD. To this end, we paired γ KC activation and
215 injection of a low concentration of forskolin. This pairing was able to induce a long-lasting
216 suppression (at least for 17 min) of the EPSC amplitude and concurrent increase in PPR (Figs.
217 3F and 3G), replicating dopamine-induced LTD. In contrast, pairing of γ KC activation with
218 injection of DMSO (0.1%; solvent of forskolin) did not show any effect (Figs. 3H and 3I). These
219 results suggest that some intracellular signal triggered by KC activity is required to converge
220 somewhere in the downstream pathway of the cAMP production to express presynaptic LTD.

221 **Dopamine-induced LTD depends on PKA but not calcium/calmodulin-dependent protein**
222 **kinase II (CaMKII)**

223 Our results so far demonstrated that cAMP pathway is a critical molecular basis for LTD, even
224 though its activation alone may not be sufficient. We therefore tested pharmacologically which
225 molecules downstream of cAMP are required for LTD induction (Fig. 4A). As with many other
226 organisms, PKA plays a crucial role in *Drosophila* olfactory learning (Drain *et al.*, 1991;
227 Skoulakis *et al.*, 1993). However, its role in the LTD at the KC output synapse has not been
228 examined. To test this, we bath-applied a PKA inhibitor H-89 (10 μM). H-89 itself did not affect

229 the EPSC amplitude or PPR but completely blocked the LTD induced by γ KC-dopamine pairing
230 (Figs. 4B and 4C). As shown in Figs. 2K and 2L, bath application of the solvent alone did not
231 show any effect. CaMKII is another protein kinase that has a conserved role in synaptic plasticity
232 across species (Bayer & Schulman, 2019). In *Drosophila*, it is also implicated in some form of
233 associative learning other than olfactory learning (Griffith *et al.*, 1993). Since our results suggest
234 an important role of KC activity, which may lead to CaMKII activation via calcium influx, we
235 tested the effect of a CaMKII inhibitor KN-93, which is effective in *Drosophila* (Peretz *et al.*,
236 1998). However, in the presence of KN-93 (10 μM), γ KC-dopamine pairing induced robust, or
237 even more pronounced, LTD and PPR increases (Figs. 4D and 4E). Since application of KN-93
238 itself slightly decreased the EPSC amplitude (but not PPR), phosphorylation by CaMKII may
239 play a role in maintaining normal synaptic transmission, perhaps on the postsynaptic side. Taken
240 together, dopamine-induced LTD in γ KCs depends on PKA, but CaMKII activation is not
241 critical for this form of synaptic plasticity.

242 **Simultaneous activation of cGMP pathway and γ KCs induces presynaptic LTP**

243 A behavioral study in dopamine-deficient flies (i.e. the mutant flies that cannot synthase
244 dopamine in neurons) identified NO as a cotransmitter of a subset of DANs (Aso *et al.*, 2019).
245 Since pairing of odor presentation and optogenetic activation of those DANs in dopamine-
246 deficient flies induced memories with opposite valence to normal flies, it has been hypothesized
247 that cGMP pathway downstream of NO induces synaptic potentiation and opposes dopamine-
248 induced LTD. To test this hypothesis, we used sGC agonist BAY 41-2272 (Fig. 5A), which can
249 activate the *Drosophila* sGC consisting of Gycα99B/Gycβ100B subunits (Morton *et al.*, 2005)
250 expressed in KCs (Fig. S1) (Aso *et al.*, 2019). When 1-min focal injection of BAY 41-2272 (100
251 μM) was repeated three times, it slowly potentiated the γ KC-to-MBON-γ1pedc synaptic
252 transmission over ~15 min in some cells, but this effect was not highly consistent between cells
253 (Figs. 5B and 5C). This variable potentiation was not accompanied by a change in PPR. In
254 contrast, when the same BAY 41-2272 injection pattern was paired with γ KC activation, we
255 reproducibly observed slowly developing LTP with concurrent decrease in PPR (Figs. 5D and
256 5E). Thus, as reminiscent of the role of cAMP pathway in LTD, it requires simultaneous KC
257 stimulation for activation of cGMP pathway to induce presynaptic plasticity, but the direction of
258 plasticity is opposite to the one induced by cAMP. Of note, our preliminary attempt with one

259 time 1-min pairing of BAY 41-2272 injection with γ KC activation did not induce LTP (n = 2;
260 data not shown). The requirement of multiple rounds of pairing for LTP induction and the slow
261 kinetics of LTP are consistent with the behavioral study that showed that NO-dependent learning
262 requires longer training than dopamine-dependent one and that NO-dependent memory develops
263 slowly over time, taking ~10 min after training (Aso *et al.*, 2019).

264 **Depression at α/β KC-to-MBON-γ1pedc synapses is short lasting**

265 In our plasticity induction method, odor-evoked KC activation, which occurs across all KC
266 subtypes, is substituted with subtype-specific optogenetic activation. This feature allowed us to
267 compare the properties of synaptic plasticity between different subtypes of KCs that share the
268 same postsynaptic MBON. To test if the α/β KC-to-MBON-γ1pedc synapses undergo similar
269 long-term synaptic plasticity to γ KC-to-MBON-γ1pedc synapses, we next expressed
270 CsChrimson in a subset of α/β KCs using α/β KC-specific split-GAL4 driver MB008C (Aso *et*
271 *al.*, 2014*b*) and the SPARC system (Fig. 6A). As with the case of γ KCs, activation of α/β KCs
272 paired with focal dopamine injection caused LTD with a concurrent increase in PPR (Figs. 6B
273 and 6C). However, the duration of LTD was markedly shorter. The EPSC amplitude as well as
274 PPR started showing recovery within 5 min after induction, and both became indistinguishable
275 from the baseline after ~10 min. In contrast, at γ KC-to-MBON-γ1pedc synapses, LTD lasted at
276 least for 30 min. Dopamine injection (Figs. 6D and 6E) or α/β KC activation (Figs. 6F and 6G)
277 alone did not induce any plasticity. These results indicate that the properties of dopamine-
278 induced synaptic plasticity are different between KC subtypes even among the synapses on the
279 same MBON.

280 To test whether difference in the duration of plasticity also applies to LTD induced by direct
281 activation of AC, we next injected forskolin (Fig. 7A). Neither a low (10 μM; Figs. 7B and 7C)
282 nor a high (100 μM; Figs. 7D and 7E) concentration of forskolin induced robust LTD or parallel
283 increase in PPRs. In contrast, when we paired injection of a low concentration of forskolin with
284 activation of α/β KCs, we observed transient but robust LTD accompanying parallel increase in
285 PPRs (Figs. 7F and 7G). Thus, as with the case of γ KCs, elevation of cAMP level by AC
286 activation is not sufficient to induce LTD at α/β KC-to-MBON-γ1pedc synapses, as it
287 additionally requires KC activation. On the other hand, the duration of LTD induced by α/β KC-

288 forskolin pairing was reminiscent of that induced by α/β KC-dopamine pairing. To exclude the
289 possibility that the short duration of LTD reflects insufficient diffusion of forskolin into the
290 pedunculus subregion, where α/β KC-to-MBON-γ1pedc synapses are located, we repeated the
291 same pairing experiment with a high concentration of forskolin (100 μM). The results mirrored
292 those with the lower concentration; LTD and accompanying increase in PPRs were robust but
293 still transient (Figs. 7H and 7I). Pairing of α/β KC activation with injection of DMSO (0.1%) did
294 not show any effect (Figs. 7J and 7K). These results confirm the short-lasting nature of cAMP-
295 induced LTD at α/β KC-to-MBON-γ1pedc synapses.

296 In contrast, cGMP-induced plasticity appeared similar between KC subtypes (Fig. 8A). As
297 observed at γ KC synapses, three times 1-min injection of BAY 41-2272 alone did not induce
298 LTP paralleled by PPR change at α/β KC-to-MBON-γ1pedc synapses (Figs. 8B and 8C). Pairing
299 of α/β KC activation and BAY 41-2272 injection induced robust LTP with a concurrent decrease
300 of PPR, which slowly developed over the period of ~10 min (Figs. 8D and 8E), again replicating
301 the observation in γ KCs. Taken together, γ and α/β KCs may share similar induction
302 mechanisms of cyclic nucleotide-induced synaptic plasticity but exhibit distinct durations
303 specifically for cAMP-dependent plasticity.

304 **Discussion**

305 In many species, brain areas and cell types, activation of cAMP/PKA pathway has been almost
306 exclusively implicated in potentiation rather than depression of synapses in the context of
307 synaptic plasticity. In this study, we provide the direct evidence that the output synapse of the
308 *Drosophila* MB is a rare, if not the only, exception where the sign of cAMP-induced plasticity is
309 inverted. Our results show that potentiation is instead mediated by cGMP pathway. Against
310 prevailing working model, increase in neither of the cyclic nucleotides was sufficient to induce
311 presynaptic plasticity; it additionally required simultaneous neuronal activity. Our experimental
312 design also allowed for a separate interrogation of synaptic plasticity exhibited by different
313 presynaptic cell types and uncovered similar but distinct properties.

314 Like in many sensory cortical areas, KCs show sparse sensory representations (Turner *et al.*,
315 2008; Honegger *et al.*, 2011). For this representation format to benefit the stimulus specificity of
316 learning (Field, 1994; Olshausen & Field, 2004), the effect of neuromodulation must be
317 restricted to the small fraction of synapses participating the sensory representation. This requires
318 synaptic plasticity to be induced only when neuromodulatory input coincides with synaptic
319 activity. Calcium/calmodulin-activated AC has been long postulated as a molecular basis for
320 such coincidence detection in multiple organisms because of its dual sensitivity to calcium influx
321 triggered by neuronal activity and G protein signaling triggered by neuromodulatory input (Mons
322 *et al.*, 1999; Heisenberg, 2003). In *Drosophila* MB, multiple studies have indeed observed
323 synergistic action of KC activity and DAN activation (or bath-applied dopamine) on the
324 cAMP/PKA pathway in the KC axons (Tomchik & Davis, 2009; Gervasi *et al.*, 2010; Handler *et*
325 *al.*, 2019). However, these and other studies also showed that DAN activation or dopamine
326 application alone can induce considerable increase in cAMP level (Tomchik & Davis, 2009; Boto
327 *et al.*, 2014; Handler *et al.*, 2019). Moreover, DAN activity is strongly modulated by the animal's
328 instantaneous locomotion (Cohn *et al.*, 2015; Siju *et al.*, 2020; Zolin *et al.*, 2021; Marquis &
329 Wilson, 2022). Thus, the resulting "aberrant" fluctuation of the cAMP level may prevent it from
330 being a faithful biochemical reporter of coincidence. Furthermore, a recent study squarely
331 challenged the role of cAMP as a coincidence reporter by showing that odor-electric shock
332 pairing evoked a similar degree of cAMP elevation in the KC axons regardless of their
333 responsiveness to the odor (Abe *et al.*, 2023). These results collectively suggest that it would be
334 problematic if cAMP increase is sufficient to induce synaptic plasticity as assumed in the
335 currently prevailing view (Heisenberg, 2003). That is, without another layer of coincidence
336 detection, synapse specificity of plasticity would be compromised. Our results indicate the
337 existence of such a mechanism. Activation of AC alone by focal application of forskolin at the
338 synaptic site failed to induce LTD. Forskolin injection at a high concentration (100 μM) did
339 induce LTD, but this LTD did not accompany a change in PPR. We speculate that excessive
340 concentration of forskolin may have recruited AC in the MBON to induce postsynaptic LTD.
341 This idea is supported by the fact that the MBON has a much lower level of AC expression
342 compared to KCs (Fig. S1). However, the lack of a change in PPR alone is not enough to specify
343 the site of the plasticity; we were unable to analyze the miniature EPSCs, the size of which could
344 have provided more mechanistic insight, due their small size. Regardless of the origin of the

345 plasticity, we can firmly conclude that the LTD induced by high concentration of forskolin is
346 qualitatively distinct from that induced by KC-dopamine pairing because only the latter showed
347 clear increase in PPR. In contrast to our results, a recent study reported that forskolin treatment
348 (100 μM) alone is sufficient to induce suppression of acetylcholine release from KCs (Abe *et al.*,
349 2023). However, this study used bath application of forskolin, and acetylcholine release was
350 evoked by an odor. Thus, the observed effect could be the result of forskolin's action on any part
351 of the upstream circuit of the KCs. Moreover, they observed that the depression induced by
352 forskolin quickly disappeared after washing out forskolin, suggesting that it is not LTD. In
353 contrast, we focally applied forskolin only to a limited area of the MB lobes. In this small area,
354 the resident MBON and DAN show much lower expression levels of AC compared to KCs (Fig.
355 S1), making it unlikely that the observed effect of forskolin is mediated by non-KC cell types.
356 Moreover, the depression induced by KC-dopamine pairing lasted for at least 30 min after
357 forskolin was washed out from the area. We were able to replicate the LTD induced by KC-
358 dopamine pairing only when focal forskolin application was paired with KC activation. Taken
359 together, we propose a model that the convergence point of the signal triggered by KC activity
360 and that by dopamine input resides somewhere downstream of the cAMP synthesis. This view
361 and the traditional view of AC as a coincidence detector are not mutually exclusive as KC
362 activity may have a dual role at both convergence points. This double-layered mechanism of
363 coincidence detection could help secure the synapse specificity of plasticity (hence stimulus
364 specificity of learning) and prevent the synapses from undergoing plasticity every time the
365 cAMP level is affected by ongoing DAN activity. It would be important to understand the signal
366 mediating the neuronal activity and the detailed molecular mechanism of the downstream
367 convergence, especially given the fact that the direction of cAMP-induced plasticity is opposite
368 to many other systems. Our results suggest that PKA but not CaMKII is involved in this process.

369 Bidirectional synaptic plasticity has been reported in KC-to-MBON-γ4 synapses, where the
370 direction of the plasticity is determined by the temporal order of KC and DAN activation
371 (Handler *et al.*, 2019). DAN activation in the absence of KC activity is also reported to
372 strengthen the MBON response (Cohn *et al.*, 2015; Berry *et al.*, 2018). Our results demonstrate
373 the presence of another format of synaptic potentiation mediated by cGMP. The direction of the
374 plasticity, higher threshold for plasticity induction, and slow kinetics of plasticity development

375 we observed match the expectation from the behavioral study that identified NO as a
376 cotramsmitter of a subset of DANs (Aso *et al.*, 2019). Since the DANs expressing NO synthase
377 are paired up with the MBONs implicated in short-term memory, it has been proposed that NO-
378 induced plasticity antagonizes dopamine-induced plasticity to shorten the memory retention
379 time. However, it is not clear whether these two plasticity pathways target the same presynaptic
380 machinery to change the synaptic strength or exist in parallel. Just like the cAMP pathway,
381 cGMP pathway also needs simultaneous neuronal activity to trigger the presynaptic plasticity. To
382 understand the detailed interaction of these two pathways, the downstream molecular target
383 needs to be identified. Recent study reported that NO-dependent cGMP signaling can trigger
384 transcriptional changes in KCs, which are essential for forgetting of memory at 6 hours after
385 training (Takakura *et al.*, 2023). Thus, the antagonistic relationship between cAMP and cGMP
386 second-messenger pathways controls memory acquisition and retention over multiple timescales
387 spanning minutes to hours to days.

388 By taking advantage of our experimental design that allows for subtype-specific activation of
389 KCs, we showed that the synapses made by α/β KCs on MBON-γ1pedc display shorter
390 dopamine-induced LTD compared to the ones made by γ KCs on the same postsynaptic neuron.
391 This result may be somewhat unexpected because the output of α/β KCs is generally considered
392 to be important for long-term memory retrieval (Isabel *et al.*, 2004; Krashes & Waddell, 2008;
393 Trannoy *et al.*, 2011; Huang *et al.*, 2013). It is unlikely, however, that the observed difference
394 between α/β KCs and γ KCs is caused by incomplete diffusion of the injected reagents because
395 we confirmed that the signal of Texas Red-conjugated dextran infused in the injection pipette
396 covers the entire γ1pedc region. In addition, the duration of LTD induced by pairing of α/β KC
397 activation with 10 μM forskolin did not change even if we used 100 μM forskolin. Furthermore,
398 the time course of cGMP-induced LTP was similar between α/β KCs and γ KCs. Thus, we
399 conclude that the difference reflects the different properties of the synapses. It is possible that
400 properties of synapses in the pedunculus region, which is an uncommon area for KCs to make
401 synapses with MBONs, are somewhat different from those of typical synapses in the MB lobes.
402 Alternatively, it is also possible that the plasticity properties observed at α/β KCs-to-MBON-
403 γ1pedc synapses generally apply to all synapses made by α/β KCs. Transcription levels of some
404 of the PKA isoforms are markedly lower in α/β KCs than in γ KCs (Fig. S1), which might

405 explain the difference. Importantly, the study using *in vivo* pairing of odor presentation and
406 optogenetic DAN activation revealed that induction of LTD in MBON-α2sc took longer pairing
407 than that in MBON-γ1 (Hige *et al.*, 2015). Thus, it is possible that the shorter LTD in α/β KCs-
408 to-MBON-γ1pedc synapses reflects higher threshold of plasticity induction in α/β KCs. It
409 requires recording from other types of MBONs with various pairing parameters to discriminate
410 these potential scenarios.

411 For a long time, the learning and memory field in *Drosophila* has been strongly driven by
412 behavioral genetics studies, which successfully made links between key molecules and
413 behavioral defects. However, the link between those molecules and their potential roles in
414 synaptic plasticity has not been extensively tested. In the rodent learning and memory field, a
415 series of experiments using slice physiology provided countless key insight into the molecular
416 and physiological basis of long-term synaptic plasticity. Our *ex vivo* system developed in this
417 study provides an equivalent platform to interrogate the molecular machinery of synaptic
418 plasticity in this historically important model organism.

419 **Material and Methods**

420 **Flies**

421 All fly stocks were maintained at room temperature on conventional cornmeal-based medium.
422 However, in most cases, we kept the final crosses for experiments in the dark at 18 °C to
423 minimize the potential phototoxicity on KCs expressing CsChrimson. Flies were selected for
424 desired genotypes on the day of eclosion, transferred to all-trans-retinal food (0.5 mM) and used
425 for experiments after 48-72 hours. For experiments to record γ KC-to-MBON-γ1pedc synaptic
426 currents (Figs. 1-5), we used *nSyb-IVS-phiC31 attp18/w; 20XUAS-SPARC2-S-Syn21-*
427 *CsChrimson::tdTomato-3.1 CR-P40/R12G04-LexA attP40; MB623C/pJFRC57-13XLexAop2-*
428 *IVS-GFP-p10 VK00005*. For α/β KC-to-MBON-γ1pedc synapses (Figs. 6-8), we used *MB008C*
429 instead of *MB623C*. *nSyb-IVS-phiC31 attp18* and *20XUAS-SPARC2-S-Syn21-*
430 *CsChrimson::tdTomato-3.1 CR-P40* flies were obtained from the Bloomington Drosophila Stock
431 Center, and MB623C flies were gifted from Yoshinori Aso (Janelia, HHMI).

432 **Electrophysiology**

433 We first attempted to perform all experiments *in vivo*. However, light stimulation we used for
434 optogenetic activation of KCs evoked an EPSC-like inward current in MBON-γ1pedc as well as
435 many of the randomly selected neurons in flies without CsChrimson transgene (data not shown).
436 These responses persisted even in the presence of tetrodotoxin (1 μM), but they almost
437 disappeared in blind *norpA* mutants and were completely absent when we removed the retina.
438 We therefore decided to switch to the *ex vivo* preparation. This strategy also improved the
439 recording condition by minimizing the spontaneous circuit activity.

440 We dissected out a brain from a head capsule in ice-cold external saline, which contains (in mM)
441 103 NaCl, 3 KCl, 1.5 $CaCl_2$, 4 $MgCl_2$, 26 $NaHCO_3$, 5 N-[tris(hydroxymethyl)-methyl]-2-
442 aminoethane-sulfonic acid, 1 NaH_2PO_4, 10 trehalose and 10 glucose (pH 7.3 when bubbled with
443 95% O_2 and 5% CO_2, 275 mOsm), and then transferred it to a recording chamber, where the
444 brain was pinned to the Sylgard-coated bottom using sharpened tungsten rods inserted at the
445 optic lobes. In some experiments, we treated the brain with Type IV collagenase (0.2-0.5 mg/ml)
446 for 30-90 s to make it easier to remove the glial sheath. After removing the sheath around the
447 region of interest by forceps and pipettes under an upright microscope (OpenStand; Prior
448 Scientific) equipped with a 60× water-immersion objective (LUMPlanFl/IR; Olympus), we
449 inserted an injection pipette containing external saline with Texas Red-conjugated dextran (3,000
450 MW; 100-200 μM) and additional drugs as described in each figure legend. The tip of injection
451 pipette was placed near the dendritic region of MBON-γ1pedc under the guidance of the GFP
452 signal in the MBON. Both injection and patch pipettes were made from borosilicate glass
453 capillaries with filament (Sutter Instrument) by a micropipette puller (P-97, Sutter Instrument).
454 Patch pipettes were further heat-polished at the tip and had a resistance of 3.5-5.5 MΩ. Pipettes
455 with a slightly larger tip diameter were used as injection pipettes. Patch pipettes were filled with
456 internal saline containing (in mM) 140 cesium aspartate, 10 HEPES, 1 EGTA, 1 KCl, 4 Mg-ATP,
457 0.5 Na-GTP and 10 QX-314 (pH adjusted to 7.3 with CsOH, 265 mOsm). Whole-cell voltage-
458 clamp recordings were made from MBON-γ1pedc using Axon MultiClamp 700B amplifier
459 (Molecular Probes). Cells were held at −60 mV. Leak current was typically < 150 pA. Series
460 resistance was compensated up to 70% so that the uncompensated component remains constant

461 at around 5 MΩ. Signals were low-pass filtered at 5 kHz before being digitized at 10 kHz.
462 Sample traces shown in figures were further low-pass filtered.

463 KCs were stimulated by 1-ms light pulses delivered through the objective at 4.25 mW/mm^2 by a
464 high-power LED source (LED4D067; Thorlabs) equipped with 625 nm LED. To measure PPR,
465 we first recorded a single-pulse EPSC to be used as a reference trace. After 10 s, we delivered 4
466 paired pulses with 400-ms intervals every 10 s. We repeated this set every minute. A second
467 EPSC waveform was obtained every minute by subtracting a reference trace from the average of
468 4 paired-pulse EPSCs. PPR was then calculated every minute by dividing the second EPSC
469 amplitude by the first EPSC amplitude. To ensure the stability of response, we recorded baseline
470 responses for at least 3 min. For focal injection of drugs, we applied 1-s pressure pulses (0.4-0.6
471 psi) every 2 s for 1 min by a microinjector (PV850, World Precision Instruments). In some
472 experiments, we repeated it three times with 1-min intervals. When we paired KC activation with
473 focal injection, photostimuli were delivered at 2 Hz for 1 min with the first pulse delivered 0.3 s
474 before the onset of the first injection pulse. Recording was resumed 2.5 min after the end of
475 injection. For bath application of drugs, we waited for 2 min after the normal bath saline was
476 exchanged with the one containing a drug via perfusion. We then recorded EPSCs for 3 min to
477 assess the effect of the drug itself before starting the pairing procedure described above. All
478 stimulus delivery and data acquisition were controlled by custom MATLAB (Mathworks) codes.
479 Data analyses were also performed on MATLAB. Statistical analyses were performed on
480 MATLAB or Prism (GraphPad). All statistical tests used raw data before normalization.

481 **Drugs**

482 Drug-containing external saline was freshly prepared on the day of experiment from stock
483 solutions stored at −20 ºC. Stock solutions of mecamylamine and KN-93 phosphate were made
484 with water at 100 mM, and SCH 23390, forskolin, H-89 and BAY 41-2272 were dissolved in
485 DMSO at 100 mM. Final concentration of DMSO did not exceed 0.1%. Dopamine was stored at
486 100 mM in external saline. When a drug was bath applied, that drug was also included in the
487 injection pipette at the same concentration.

488 **Acknowledgements**

489 We thank Yoshinori Aso and members of the Hige lab for valuable comments on the manuscript.
490 This work was supported by grants from National Institutes of Health (R01DC018874), National
491 Science Foundation (2034783) and United States-Israel Binational Science Foundation
492 (2019026) awarded to TH. DY was supported by Toyobo Biotechnology Foundation
493 Postdoctoral Fellowship and Japan Society for the Promotion of Science Overseas Research
494 Fellowship. Stocks obtained from FlyLight Split-GAL4 Driver Collection (Janelia, HHMI) and
495 the Bloomington Drosophila Stock Center (NIH P40OD018537) were used in this study.

496 **References**

497 Abe T, Yamazaki D, Hiroi M, Ueoka Y, Maeyama Y & Tabata T (2023). Revisiting the role of
498 cAMP in Drosophila aversive olfactory memory formation. 2023.06.26.545795.
499 Available at: https://www.biorxiv.org/content/10.1101/2023.06.26.545795v1.

500 Akalal D-BG, Yu D & Davis RL (2010). A late-phase, long-term memory trace forms in the γ
501 neurons of Drosophila mushroom bodies after olfactory classical conditioning. *J Neurosci*
502 **30,** 16699–16708.

503 Arancio O, Kandel ER & Hawkins RD (1995). Activity-dependent long-term enhancement of
504 transmitter release by presynaptic 3′,5′-cyclic GMP in cultured hippocampal neurons.
505 *Nature* **376,** 74–80.

506 Aso Y et al. (2014*a*). Mushroom body output neurons encode valence and guide memory-based
507 action selection in Drosophila. *eLife* **3,** e04580.

508 Aso Y, Hattori D, Yu Y, Johnston RM, Iyer NA, Ngo T-TB, Dionne H, Abbott LF, Axel R,
509 Tanimoto H & Rubin GM (2014*b*). The neuronal architecture of the mushroom body
510 provides a logic for associative learning. *eLife* **3,** e04577.

511 Aso Y, Ray RP, Long X, Bushey D, Cichewicz K, Ngo T-T, Sharp B, Christoforou C, Hu A,
512 Lemire AL, Tillberg P, Hirsh J, Litwin-Kumar A & Rubin GM (2019). Nitric oxide acts as
513 a cotransmitter in a subset of dopaminergic neurons to diversify memory dynamics. *eLife*
514 **8,** e49257.

515 Aso Y & Rubin GM (2016). Dopaminergic neurons write and update memories with cell-type-
516 specific rules. *eLife* **5,** e16135.

517 Awata H, Takakura M, Kimura Y, Iwata I, Masuda T & Hirano Y (2019). The neural circuit
518 linking mushroom body parallel circuits induces memory consolidation in Drosophila.
519 *Proc Natl Acad Sci* **116,** 16080–16085.

520 Bayer KU & Schulman H (2019). CaM Kinase: Still Inspiring at 40. *Neuron* **103,** 380–394.

521 Berry JA, Phan A & Davis RL (2018). Dopamine Neurons Mediate Learning and Forgetting
522 through Bidirectional Modulation of a Memory Trace. *Cell Rep* **25,** 651-662.e5.

523 Blum AL, Li W, Cressy M & Dubnau J (2009). Short- and long-term memory in Drosophila
524 require cAMP signaling in distinct neuron types. *Curr Biol* **19,** 1341–1350.

525 Boto T, Louis T, Jindachomthong K, Jalink K & Tomchik SM (2014). Dopaminergic modulation
526 of cAMP drives nonlinear plasticity across the Drosophila mushroom body lobes. *Curr*
527 *Biol* **24,** 822–831.

528 Britt JP, Benaliouad F, McDevitt RA, Stuber GD, Wise RA & Bonci A (2012). Synaptic and
529 Behavioral Profile of Multiple Glutamatergic Inputs to the Nucleus Accumbens. *Neuron*
530 **76,** 790–803.

531 Brunelli M, Castellucci V & Kandel ER (1976). Synaptic Facilitation and Behavioral
532 Sensitization in Aplysia: Possible Role of Serotonin and Cyclic AMP. *Science* **194,** 1178–
533 1181.

534 Burke CJ, Huetteroth W, Owald D, Perisse E, Krashes MJ, Das G, Gohl DM, Silies M, Certel S
535 & Waddell S (2012). Layered reward signalling through octopamine and dopamine in
536 Drosophila. *Nature* **492,** 433–437.

537 Byers D, Davis RL & Kiger JA (1981). Defect in cyclic AMP phosphodiesterase due to the dunce
538 mutation of learning in Drosophila melanogaster. *Nature* **289,** 79–81.

539 Calabresi P, Gubellini P, Centonze D, Sancesario G, Morello M, Giorgi M, Pisani A & Bernardi
540 G (1999). A Critical Role of the Nitric Oxide/cGMP Pathway in Corticostriatal Long-
541 Term Depression. *J Neurosci* **19,** 2489–2499.

542 Caplan SL, Milton SL & Dawson-Scully K (2013). A cGMP-dependent protein kinase (PKG)
543 controls synaptic transmission tolerance to acute oxidative stress at the Drosophila larval
544 neuromuscular junction. *J Neurophysiol* **109,** 649–658.

545 Castellucci VF, Kandel ER, Schwartz JH, Wilson FD, Nairn AC & Greengard P (1980).
546 Intracellular injection of the catalytic subunit of cyclic AMP-dependent protein kinase
547 simulates facilitation of transmitter release underlying behavioral sensitization in Aplysia.
548 *Proc Natl Acad Sci* **77,** 7492–7496.

549 Chevaleyre V, Heifets BD, Kaeser PS, Südhof TC & Castillo PE (2007). Endocannabinoid-
550 Mediated Long-Term Plasticity Requires cAMP/PKA Signaling and RIM1α. *Neuron* **54,**
551 801–812.

552 Cohn R, Morantte I & Ruta V (2015). Coordinated and Compartmentalized Neuromodulation
553 Shapes Sensory Processing in Drosophila. *Cell* **163,** 1742–1755.

554 Creed M, Ntamati NR, Chandra R, Lobo MK & Lüscher C (2016). Convergence of Reinforcing
555 and Anhedonic Cocaine Effects in the Ventral Pallidum. *Neuron* **92,** 214–226.

556 Drain P, Folkers E & Quinn WG (1991). cAMP-dependent protein kinase and the disruption of
557 learning in transgenic flies. *Neuron* **6,** 71–82.

558 Felsenberg J, Jacob PF, Walker T, Barnstedt O, Edmondson-Stait AJ, Pleijzier MW, Otto N,
559 Schlegel P, Sharifi N, Perisse E, Smith CS, Lauritzen JS, Costa M, Jefferis GSXE, Bock
560 DD & Waddell S (2018). Integration of Parallel Opposing Memories Underlies Memory
561 Extinction. *Cell* **175,** 709-722.e15.

562 Field DJ (1994). What Is the Goal of Sensory Coding? *Neural Comput* **6,** 559–601.

563 Gervasi N, TchEnio P & Preat T (2010). PKA Dynamics in a Drosophila Learning Center:
564 Coincidence Detection by Rutabaga Adenylyl Cyclase and Spatial Regulation by Dunce
565 Phosphodiesterase. *Neuron* **65,** 516–529.

566 Goldsmith BA & Abrams TW (1991). Reversal of synaptic depression by serotonin at Aplysia
567 sensory neuron synapses involves activation of adenylyl cyclase. *Proc Natl Acad Sci* **88,**
568 9021–9025.

569 Griffith LC, Verselis LM, Aitken KM, Kyriacou CP, Danho W & Greenspan RJ (1993).
570 Inhibition of calcium/calmodulin-dependent protein kinase in drosophila disrupts
571 behavioral plasticity. *Neuron* **10,** 501–509.

572 Hancock CE, Rostami V, Rachad EY, Deimel SH, Nawrot MP & Fiala A (2022). Visualization of
573 learning-induced synaptic plasticity in output neurons of the Drosophila mushroom body
574 γ-lobe. *Sci Rep* **12,** 10421.

575 Handler A, Graham TGW, Cohn R, Morantte I, Siliciano AF, Zeng J, Li Y & Ruta V (2019).
576 Distinct Dopamine Receptor Pathways Underlie the Temporal Sensitivity of Associative
577 Learning. *Cell* **178,** 60-75.e19.

578 Heisenberg M (2003). Mushroom body memoir: from maps to models. *Nat Rev Neurosci* **4,** 266–
579 275.

580 Hige T, Aso Y, Modi MN, Rubin GM & Turner GC (2015). Heterosynaptic Plasticity Underlies
581 Aversive Olfactory Learning in Drosophila. *Neuron* **88,** 985–998.

582 Honegger KS, Campbell RAA & Turner GC (2011). Cellular-Resolution Population Imaging
583 Reveals Robust Sparse Coding in the Drosophila Mushroom Body. *J Neurosci* **31,**
584 11772–11785.

585 Huang C, Wang P, Xie Z, Wang L & Zhong Y (2013). The differential requirement of mushroom
586 body α/β subdivisions in long-term memory retrieval in Drosophila. *Protein Cell* **4,** 512–
587 519.

588 Huang Y-Y, Li X-C & Kandel ER (1994). cAMP contributes to mossy fiber LTP by initiating
589 both a covalently mediated early phase and macromolecular synthesis-dependent late
590 phase. *Cell* **79,** 69–79.

591 Isaacman-Beck J, Paik KC, Wienecke CFR, Yang HH, Fisher YE, Wang IE, Ishida IG, Maimon
592 G, Wilson RI & Clandinin TR (2020). SPARC enables genetic manipulation of precise
593 proportions of cells. *Nat Neurosci* **98,** 256–258.

594 Isabel G, Pascual A & Preat T (2004). Exclusive consolidated memory phases in Drosophila.
595 *Science* **304,** 1024–1027.

596 Kandel ER, Dudai Y & Mayford MR (2014). The Molecular and Systems Biology of Memory.
597 *Cell* **157,** 163–186.

598 Kim YC, Lee HG & Han K-AA (2007). D1 Dopamine Receptor dDA1 Is Required in the
599 Mushroom Body Neurons for Aversive and Appetitive Learning in Drosophila. *J*
600 *Neurosci* **27,** 7640–7647.

601 Klapoetke NC et al. (2014). Independent optical excitation of distinct neural populations. *Nat*
602 *Methods* **11,** 338–346.

603 Krashes MJ & Waddell S (2008). Rapid Consolidation to a radish and Protein Synthesis-
604 Dependent Long-Term Memory after Single-Session Appetitive Olfactory Conditioning
605 in Drosophila. *J Neurosci* **28,** 3103–3113.

606 Kuromi H & Kidokoro Y (2000). Tetanic Stimulation Recruits Vesicles from Reserve Pool via a
607 cAMP-Mediated Process in Drosophila Synapses. *Neuron* **27,** 133–143.

608 Lev-Ram V, Jiang T, Wood J, Lawrence DS & Tsien RY (1997). Synergies and Coincidence
609 Requirements between NO, cGMP, and Ca2+ in the Induction of Cerebellar Long-Term
610 Depression. *Neuron* **18,** 1025–1038.

611 Lewin MR & Walters ET (1999). Cyclic GMP pathway is critical for inducing long–term
612 sensitization of nociceptive sensory neurons. *Nat Neurosci* **2,** 18–23.

613 Liu C, Plaçais P-Y, Yamagata N, Pfeiffer BD, Aso Y, Friedrich AB, Siwanowicz I, Rubin GM,
614 Preat T & Tanimoto H (2012). A subset of dopamine neurons signals reward for odour
615 memory in Drosophila. *Nature* **488,** 512–516.

616 Liu W-Z, Zhang W-H, Zheng Z-H, Zou J-X, Liu X-X, Huang S-H, You W-J, He Y, Zhang J-Y,
617 Wang X-D & Pan B-X (2020). Identification of a prefrontal cortex-to-amygdala pathway
618 for chronic stress-induced anxiety. *Nat Commun* **11,** 2221.

619 Livingstone MS, Sziber PP & Quinn WG (1984). Loss of calcium/calmodulin responsiveness in
620 adenylate cyclase of rutabaga, a Drosophila learning mutant. *Cell* **37,** 205–215.

621 Marquis M & Wilson RI (2022). Locomotor and olfactory responses in dopamine neurons of the
622 Drosophila superior-lateral brain. *Curr Biol*; DOI: 10.1016/j.cub.2022.11.008.

623 McCurdy LY, Sareen P, Davoudian PA & Nitabach MN (2021). Dopaminergic mechanism
624 underlying reward-encoding of punishment omission during reversal learning in
625 Drosophila. *Nat Commun* **12,** 1115.

626 McGuire SE, Le PT, Osborn AJ, Matsumoto K & Davis RL (2003). Spatiotemporal rescue of
627 memory dysfunction in Drosophila. *Science* **302,** 1765–1768.

628 Mons N, Guillou J-L & Jaffard R (1999). The role of Ca2+/calmodulin-stimulable adenylyl
629 cyclases as molecular coincidence detectors in memory formation. *Cell Mol Life Sci*
630 *CMLS* **55,** 525–533.

631 Morton DB, Langlais KK, Stewart JA & Vermehren A (2005). Comparison of the properties of
632 the five soluble guanylyl cyclase subunits in Drosophila melanogaster. *J Insect Sci* **5,** 1–
633 10.

634 Noyes NC & Davis RL (2023). Innate and learned odor-guided behaviors utilize distinct
635 molecular signaling pathways in a shared dopaminergic circuit. *Cell Rep* **42,** 112026.

636 Olshausen BA & Field DJ (2004). Sparse coding of sensory inputs. *Curr Opin Neurobiol* **14,**
637 481–487.

638 Owald D, Felsenberg J, Talbot CB, Das G, Perisse E, Huetteroth W & Waddell S (2015). Activity
639 of defined mushroom body output neurons underlies learned olfactory behavior in
640 Drosophila. *Neuron* **86,** 417–427.

641 Peretz A, Abitbol I, Sobko A, Wu C-F & Attali B (1998). A Ca2+/Calmodulin-Dependent Protein
642 Kinase ModulatesDrosophila Photoreceptor K+ Currents: A Role in Shaping the
643 Photoreceptor Potential. *J Neurosci* **18,** 9153–9162.

644 Perisse E, Owald D, Barnstedt O, Talbot CB, Huetteroth W & Waddell S (2016). Aversive
645 Learning and Appetitive Motivation Toggle Feed-Forward Inhibition in the Drosophila
646 Mushroom Body. *Neuron* **90,** 1086–1099.

647 Qin H, Cressy M, Li W, Coravos JS, Izzi SA & Dubnau J (2012). Gamma neurons mediate
648 dopaminergic input during aversive olfactory memory formation in Drosophila. *Curr Biol*
649 **22,** 608–614.

650 Reyes-Harde M, Empson R, Potter BVL, Galione A & Stanton PK (1999). Evidence of a role for
651 cyclic ADP-ribose in long-term synaptic depression in hippocampus. *Proc Natl Acad Sci*
652 **96,** 4061–4066.

653 Robinson SW, Bourgognon J-M, Spiers JG, Breda C, Campesan S, Butcher A, Mallucci GR,
654 Dinsdale D, Morone N, Mistry R, Smith TM, Guerra-Martin M, Challiss RAJ, Giorgini F
655 & Steinert JR (2018). Nitric oxide-mediated posttranslational modifications control
656 neurotransmitter release by modulating complexin farnesylation and enhancing its
657 clamping ability. *PLOS Biol* **16,** e2003611.

658 Salin PA, Malenka RC & Nicoll RA (1996). Cyclic AMP Mediates a Presynaptic Form of LTP at
659 Cerebellar Parallel Fiber Synapses. *Neuron* **16,** 797–803.

660 Schnitzer M, Huang C, Luo J, Woo SJ, Roitman L, Li J, Pieribone V, Kannan M & Vasan G
661 (2022). *Dopamine signals integrate innate and learnt valences to regulate memory*

dynamics. In Review. Available at: https://www.researchsquare.com/article/rs-1915648/v1.

Schwaerzel M, Monastirioti M, Scholz H, Friggi-Grelin F, Birman S & Heisenberg M (2003). Dopamine and octopamine differentiate between aversive and appetitive olfactory memories in Drosophila. *J Neurosci* **23,** 10495–10502.

Séjourné J, Plaçais P-Y, Aso Y, Siwanowicz I, Trannoy S, Thoma V, Tedjakumala SR, Rubin GM, TchEnio P, Ito K, Isabel G, Tanimoto H & Preat T (2011). Mushroom body efferent neurons responsible for aversive olfactory memory retrieval in Drosophila. *Nat Neurosci* **14,** 903–910.

Shibuki K & Okada D (1991). Endogenous nitric oxide release required for long-term synaptic depression in the cerebellum. *Nature* **349,** 326–328.

Shuai Y, Sammons M, Sterne GR, Hibbard K, Yang H, Yang C-P, Managan C, Siwanowicz I, Lee T, Rubin GM, Turner GC & Aso Y (2023). Driver lines for studying associative learning in Drosophila. 2023.09.15.557808. Available at: https://www.biorxiv.org/content/10.1101/2023.09.15.557808v1.

Siju KP, Stih V, Aimon S, Gjorgjieva J, Portugues R & Grunwald Kadow IC (2020). Valence and State-Dependent Population Coding in Dopaminergic Neurons in the Fly Mushroom Body. *Curr Biol* **30,** 2104-2115.e4.

Skoulakis EMC, Kalderon D & Davis RL (1993). Preferential expression in mushroom bodies of the catalytic subunit of protein kinase A and its role in learning and memory. *Neuron* **11,** 197–208.

Takakura M, Lam YH, Nakagawa R, Ng MY, Hu X, Bhargava P, Alia AG, Gu Y, Wang Z, Ota T, Kimura Y, Morimoto N, Osakada F, Lee AY, Leung D, Miyashita T, Du J, Okuno H & Hirano Y (2023). Differential second messenger signaling via dopamine neurons bidirectionally regulates memory retention. *Proc Natl Acad Sci* **120,** e2304851120.

Tomchik SM & Davis RL (2009). Dynamics of Learning-Related cAMP Signaling and Stimulus Integration in the Drosophila Olfactory Pathway. *Neuron* **64,** 510–521.

Trannoy S, Redt-Clouet C, Dura J-M & Preat T (2011). Parallel processing of appetitive short- and long-term memories in Drosophila. *Curr Biol* **21,** 1647–1653.

Turner GC, Bazhenov M & Laurent G (2008). Olfactory Representations by Drosophila Mushroom Body Neurons. *J Neurophysiol* **99,** 734–746.

Tzounopoulos T, Janz R, Südhof TC, Nicoll RA & Malenka RC (1998). A Role for cAMP in Long-Term Depression at Hippocampal Mossy Fiber Synapses. *Neuron* **21,** 837–845.

Wang Y, Mamiya A, Chiang A-S s & Zhong Y (2008). Imaging of an Early Memory Trace in the Drosophila Mushroom Body. *J Neurosci* **28,** 4368–4376.

698 Wildemann B & Bicker G (1999). Nitric oxide and cyclic GMP induce vesicle release at
699 Drosophila neuromuscular junction. *J Neurobiol* **39,** 337–346.

700 Yu D, Akalal D-BG & Davis RL (2006). Drosophila α/β Mushroom Body Neurons Form a
701 Branch-Specific, Long-Term Cellular Memory Trace after Spaced Olfactory
702 Conditioning. *Neuron* **52,** 845–855.

703 Zeng J, Li X, Zhang R, Lv M, Wang Y, Tan K, Xia X, Wan J, Jing M, Zhang X, Li Y, Yang Y,
704 Wang L, Chu J, Li Y & Li Y (2023). Local 5-HT signaling bi-directionally regulates the
705 coincidence time window for associative learning. *Neuron* **111,** 1118-1135.e5.

706 Zhang X, Noyes NC, Zeng J, Li Y & Davis RL (2019). Aversive Training Induces Both Pre- and
707 Postsynaptic Suppression in Drosophila. *J Neurosci* **39,** 9164–9172.

708 Zhong Y & Wu CF (1991). Altered synaptic plasticity in Drosophila memory mutants with a
709 defective cyclic AMP cascade. *Science* **251,** 198–201.

710 Zolin A, Cohn R, Pang R, Siliciano AF, Fairhall AL & Ruta V (2021). Context-dependent
711 representations of movement in Drosophila dopaminergic reinforcement pathways. *Nat*
712 *Neurosci* **24,** 1555–1566.

713 Zucker RS & Regehr WG (2002). Short-Term Synaptic Plasticity. *Annu Rev Physiol* **64,** 355–
714 405.

715 **Figure Legends**

716 **Figure 1. Optogenetic assessment of short-term synaptic plasticity at KC-to-MBON**
717 **synapses**

718 A, a schematic of the experiments. Optogenetically evoked EPSCs were measured at γ KC-to-
719 MBON-γ1pedc synapses by whole-cell voltage-clamp recordings from MBON-γ1pedc. Short-
720 term plasticity induced by paired pulses (pulse width, 1 ms; interval, 400 ms) was monitored
721 while changing the extracellular concentrations of divalent cations or partially blocking
722 postsynaptic ionotropic receptors.
723 B, changing the extracellular calcium/magnesium concentrations from 1.5/4 mM (normal) to
724 0.7/5.5 mM (low Ca/Mg) decreased the first EPSC amplitude (left, mean ± s.e.m; $n = 6$, $p < 10^{-4}$,
725 paired t-test) while increasing the PPR (right, $p = 0.00658$). Gray lines indicate data from
726 individual cells. Upper left traces show overlaid representative EPSCs before (black) and after
727 (red) changing the extracellular saline. Horizontal and vertical scale bars in this and the other

728 panels indicate 300 ms and 30 pA, respectively. Upper right traces show the same EPSCs
729 normalized with the first EPSC amplitude. Asterisks denote $p < 0.05$.
730 C, changing the extracellular calcium/magnesium concentrations to 5/0.5 mM (high Ca/Mg)
731 increased the first EPSC amplitude (left; $n = 5$, $p = 0.00778$, paired t-test) while decreasing the
732 PPR (right; $p < 10^{-4}$).
733 D, bath application of mecamylamine (Mec; 10 μM), a non-competitive antagonist of the
734 nicotinic acetylcholine receptors, reduced the first EPSC amplitude (left; $n = 5$, $p = 0.0144$,
735 paired t-test) without affecting the PPR (right, $p = 0.854$).

736 **Figure 2. Pairing γ KC activation with focal dopamine application induces presynaptic LTD**
737 **via D_1-like dopamine receptors**

738 A, a schematic of the experiments. Dopamine (1 mM) was focally applied to the dendritic region
739 of the MBON-γ1pedc via an injection pipette while measuring optogenetically evoked γ KC-to-
740 MBON-γ1pedc EPSCs. See Methods for detailed parameters for injections and recordings.
741 B, a representative image (lower left) to show the spread of the fluorescent signal of Texas Red
742 dextran, which was infused with dopamine in the injection pipette, after 1-min injection. Upper
743 left image shows a widefield view of the same sample. The γ lobe and part of the vertical lobes
744 are outlined by yellow. Light blue line indicates the approximate location of the γ1pedc region.
745 Signals measured in four regions of interest (light magenta squares) were plotted on the right.
746 Horizontal red bar denotes the timing of the injection. D: dorsal, L: lateral, scale bar: 20 μm.
747 C, first EPSC amplitudes (open circles, mean ± s.e.m; $n = 6$) and PPRs (filled circles) plotted
748 against time after the end of 1-min pairing of γ KC activation and dopamine injection. The data
749 were normalized to the average of a 3-min baseline recorded before pairing. Upper right traces
750 show overlaid representative EPSCs sampled before (at −2 min; black) and after (at 3 min; red)
751 pairing. Horizontal and vertical scale bars in this and the other panels indicate 300 ms and 30 pA,
752 respectively. Lower right traces show the same EPSCs normalized with the first EPSC
753 amplitude.
754 D, quantification of the data shown in C at early, middle and late periods after pairing (mean ±
755 s.e.m.). Black dots indicate data from individual cells. First EPSC amplitudes (open bars) and
756 PPRs (filled bars) showed depression and an increase, respectively, at all three time points. P

757 values for EPSCs are (from left to right) $< 10^{-3}$, $< 10^{-3}$ and $< 10^{-3}$ (Dunnett's multiple
758 comparisons test following repeated measures one-way ANOVA, $p < 10^{-3}$), and for PPRs, $< 10^{-3}$,
759 $< 10^{-4}$ and $< 10^{-3}$ (repeated measures one-way ANOVA, $p < 10^{-4}$).
760 E, same as C, but KC activation was omitted during pairing (n = 5).
761 F, quantification of the data shown in E. 1-min dopamine injection alone affected neither first
762 EPSC amplitudes (p = 0.372, repeated measures one-way ANOVA) nor PPRs (p = 0.160).
763 G, same as C, but dopamine application was omitted during pairing (n = 5).
764 H, quantification of the data shown in G. 1-min KC activation alone affected neither first EPSC
765 amplitudes (p = 0.632, repeated measures one-way ANOVA) nor PPRs (p = 0.676).
766 I, same as C, but D_1-like dopamine receptor antagonist SCH 23390 (100 μM) was bath-applied
767 prior to pairing and continuously until the end of experiments (n = 5). Sample traces (right)
768 include an example recorded after application of SCH 23390 but before pairing (at −2 min; blue).
769 J, quantification of the data shown in I. Pairing was ineffective in the presence of SCH 23390,
770 while SCH 23390 alone did not affect first EPSC amplitudes (p = 0.791, repeated measures one-
771 way ANOVA) or PPRs (p = 0.464).
772 K, same as I, but instead of SCH 23390, only the solvent DMSO (0.1%) was bath-applied (n =
773 6).
774 L, quantification of the data shown in I. The effects of pairing were unaffected by DMSO, while
775 DMSO alone did not affect first EPSC amplitudes or PPRs. P values for EPSCs are (from left to
776 right) 0.973, $< 10^{-4}$, $< 10^{-4}$ and $< 10^{-4}$ (Dunnett's multiple comparisons test following repeated
777 measures one-way ANOVA, $p < 10^{-6}$), and for PPRs, 1.00, 0.00896, 0.00304 and $< 10^{-3}$
778 (repeated measures one-way ANOVA, $p < 10^{-3}$).

779 **Figure 3. Presynaptic LTD induction at γ KC-to-MBON-γ1pedc synapses requires both AC**
780 **activation and KC activity**

781 A, a schematic of the experiments. AC activator forskolin was focally applied to the dendritic
782 region of the MBON-γ1pedc via an injection pipette while measuring optogenetically evoked γ
783 KC-to-MBON-γ1pedc EPSCs.
784 B, first EPSC amplitudes (open circles, mean ± s.e.m; n = 7) and PPRs (filled circles) plotted
785 against time after the end of 1-min injection of forskolin (20 μM). The data were normalized to
786 the average of a 3-min baseline recorded before pairing. Upper right traces show overlaid

787 representative EPSCs sampled before (at −2 min; black) and after (at 3 min; red) injection.
788 Horizontal and vertical scale bars in this and the other panels indicate 300 ms and 30 pA,
789 respectively. Lower right traces show the same EPSCs normalized with the first EPSC
790 amplitude.
791 C, quantification of the data shown in B at early, middle and late periods after injection (mean ±
792 s.e.m.). Black dots indicate data from individual cells. 1-min injection of a low concentration of
793 forskolin alone affected neither first EPSC amplitudes (open bars; $p = 0.0866$, repeated measures
794 one-way ANOVA) nor PPRs (filled bars; $p = 0.553$).
795 D, same as B, but with a higher concentration of forskolin (100 μM; $n = 7$).
796 E, quantification of the data shown in D. 1-min injection of a high concentration of forskolin
797 decreased first EPSC amplitudes at all three time points ($p = 0.0151$, 0.00645, and 0.00495 from
798 left to right, Dunnett's multiple comparisons test following repeated measures one-way ANOVA,
799 $p = 0.00502$) but did not affect PPRs ($p = 0.494$, repeated measures one-way ANOVA).
800 F, same as B, but 1-min forskolin (20 μM) injection was paired with γ KC activation ($n = 6$).
801 G, quantification of the data shown in F. 1-min pairing of a low concentration of forskolin and γ
802 KC activation depressed first EPSC amplitudes and increased PPRs at all three time points. P
803 values for EPSCs are (from left to right) $< 10^{-6}$, $< 10^{-6}$ and $< 10^{-6}$ (Dunnett's multiple
804 comparisons test following repeated measures one-way ANOVA, $p < 10^{-7}$), and for PPRs, $< 10^{-3}$,
805 $< 10^{-4}$ and 10^{-3} (repeated measures one-way ANOVA, $p < 10^{-4}$).
806 H, same as B, but instead of forskolin, only the solvent DMSO (0.1 %) was injected ($n = 5$). 1-
807 min injection was repeated 3 times with 1-min intervals so that the data could also serve as
808 control for the experiments shown in Fig. 5.
809 I, quantification of the data shown in H. DMSO injection alone did not affect first EPSC
810 amplitudes ($p = 0.908$, repeated measures one-way ANOVA) or PPRs ($p = 0.708$).

811 **Figure 4. Dopamine-induced LTD depends on PKA but not CaMKII**

812 A, a schematic of the experiments. Dopamine (1 mM) injection was paired with γ KC activation
813 while measuring optogenetically evoked γ KC-to-MBON-γ1pedc EPSCs as in Fig. 2C, except
814 kinase inhibitors were bath-applied prior to pairing and applied continuously until the end of
815 experiments.
816 B, effects of PKA inhibitor, H-89 (10 μM). First EPSC amplitudes (open circles, mean ± s.e.m; n

817 = 5) and PPRs (filled circles) plotted against time after the end of 1-min pairing of γ KC
818 activation and dopamine injection. The data were normalized to the average of a 3-min baseline
819 recorded before pairing. A horizontal blue bar indicates the period of H-89 application. Upper
820 right traces show overlaid representative EPSCs sampled before (at −7 min; black) and 4.5 min
821 after drug application (at −2 min; blue), and after pairing (at 3 min; red). Horizontal and vertical
822 scale bars in this and the other panels indicate 300 ms and 30 pA, respectively. Lower right
823 traces show the same EPSCs normalized with the first EPSC amplitude.
824 C, quantification of the data shown in B before pairing and at early, middle and late periods after
825 pairing (mean ± s.e.m.). Black dots indicate data from individual cells. H-89 alone did not affect
826 first EPSC amplitudes (open bars) or PPRs (filled bars), and the subsequent pairing did not
827 depress EPSCs ($p = 0.392$, repeated measures one-way ANOVA) or increase PPRs ($p = 0.205$,
828 0.171, 1.00 and 0.0174 from left to right, Dunnett's multiple comparisons test following repeated
829 measures one-way ANOVA, $p < 10^{-3}$).
830 D, same as B, but instead of H-89, CaMKII inhibitor KN-93 (10 μM) was bath-applied ($n = 4$).
831 E, quantification of the data shown in D. KN-93 alone slightly depressed EPSCs without
832 affecting PPRs, and the subsequent pairing further induced robust depression of EPSCs and
833 facilitation of PPRs. P values for EPSCs are (from left to right) $< 10^{-3}$, $< 10^{-9}$, $< 10^{-9}$ and $< 10^{-9}$
834 (Dunnett's multiple comparisons test following repeated measures one-way ANOVA, $p < 10^{-9}$),
835 and for PPRs, 0.984, $< 10^{-3}$, 0.00397 and $< 10^{-3}$ (repeated measures one-way ANOVA, $p < 10^{-3}$).

836 **Figure 5. Simultaneous activation of cGMP pathway and γ KCs induces presynaptic LTP**

837 A, a schematic of the experiments. sGC agonist BAY 41-2272 was focally applied to the
838 dendritic region of the MBON-γ1pedc via an injection pipette while measuring optogenetically
839 evoked γ KC-to-MBON-γ1pedc EPSCs.
840 B, first EPSC amplitudes (open circles, mean ± s.e.m; $n = 5$) and PPRs (filled circles) plotted
841 against time after the end of the three repeats of 1-min injection of BAY 41-2272 (100 μM). The
842 data were normalized to the average of a 3-min baseline recorded before pairing. Upper right
843 traces show overlaid representative EPSCs sampled before (at −6 min; black) and after (at 17
844 min; red) injection. Horizontal and vertical scale bars in this and the other panels indicate 300 ms
845 and 60 pA, respectively. Lower right traces show the same EPSCs normalized with the first
846 EPSC amplitude.

847 C, quantification of the data shown in B at early, middle and late periods after injection (mean ±
848 s.e.m.). Black dots indicate data from individual cells. BAY 41-2272 injection alone did not
849 induce consistent changes in first EPSC amplitudes (open bars; $p = 0.0633$, repeated measures
850 one-way ANOVA) or PPRs (filled bars; $p = 0.565$).
851 D, same as B, but BAY 41-2272 injection was paired with γ KC activation ($n = 5$).
852 E, quantification of the data shown in D. pairing of BAY 41-2272 and γ KC activation
853 potentiated first EPSC amplitudes and decreased PPRs at middle and late time points. P values
854 for EPSCs are (from left to right) 0.314, $< 10^{-3}$ and $< 10^{-3}$ (Dunnett's multiple comparisons test
855 following repeated measures one-way ANOVA, $p < 10^{-4}$), and for PPRs, 0.350, 0.00486 and
856 0.00902 (repeated measures one-way ANOVA, $p = 0.00553$).

857 **Figure 6. Pairing α/β KC activation with focal dopamine application induces transient**
858 **presynaptic LTD**

859 A, a schematic of the experiments. Dopamine (1 mM) was focally applied to the dendritic region
860 of the MBON-γ1pedc via an injection pipette while measuring optogenetically evoked α/β KC-
861 to-MBON-γ1pedc EPSCs.
862 B, first EPSC amplitudes (open circles, mean ± s.e.m; $n = 6$) and PPRs (filled circles) plotted
863 against time after the end of 1-min pairing of α/β KC activation and dopamine injection. The
864 data were normalized to the average of a 3-min baseline recorded before pairing. Upper right
865 traces show overlaid representative EPSCs sampled before (at −2 min; black) and after (at 3 min;
866 red) pairing. Horizontal and vertical scale bars in this and the other panels indicate 300 ms and
867 100 pA, respectively. Lower right traces show the same EPSCs normalized with the first EPSC
868 amplitude.
869 C, quantification of the data shown in B at early, middle and late periods after pairing (mean ±
870 s.e.m.). Black dots indicate data from individual cells. First EPSC amplitudes (open bars) and
871 PPRs (filled bars) showed depression and increase, respectively, but only transiently at the early
872 time point. P values for EPSCs are (from left to right) $< 10^{-4}$, 0.100 and 0.593 (Dunnett's
873 multiple comparisons test following repeated measures one-way ANOVA, $p < 10^{-4}$), and for
874 PPRs, $< 10^{-5}$, 0.253 and 0.999 (repeated measures one-way ANOVA, $p < 10^{-5}$).
875 D, same as B, but KC activation was omitted during pairing ($n = 5$).

876 E, quantification of the data shown in D. 1-min dopamine injection alone affected neither first
877 EPSC amplitudes ($p = 0.208$, repeated measures one-way ANOVA) nor PPRs ($p = 0.350$).
878 F, same as B, but dopamine application was omitted during pairing ($n = 5$).
879 G, quantification of the data shown in G. 1-min KC activation alone affected neither first EPSC
880 amplitudes ($p = 0.213$, repeated measures one-way ANOVA) nor PPRs ($p = 0.518$).

881 **Figure 7. Presynaptic LTD induction at α/β KC-to-MBON-γ1pedc synapses requires both**
882 **AC activation and KC activity**

883 A, a schematic of the experiments. Forskolin was focally applied to the dendritic region of the
884 MBON-γ1pedc via an injection pipette while measuring optogenetically evoked α/β KC-to-
885 MBON-γ1pedc EPSCs.
886 B, first EPSC amplitudes (open circles, mean ± s.e.m; $n = 6$) and PPRs (filled circles) plotted
887 against time after the end of 1-min injection of forskolin (10 μM). The data were normalized to
888 the average of a 3-min baseline recorded before pairing. Upper right traces show overlaid
889 representative EPSCs sampled before (at −2 min; black) and after (at 3 min; red) injection.
890 Horizontal and vertical scale bars indicate 300 ms and 100 pA, respectively. Lower right traces
891 show the same EPSCs normalized with the first EPSC amplitude.
892 C, quantification of the data shown in B at early and late periods after injection (mean ± s.e.m.).
893 Black dots indicate data from individual cells. 1-min injection of a low concentration of forskolin
894 alone did not induce consistent changes in first EPSC amplitudes (open bars; $p = 0.999$ and
895 0.0119 from left to right, Dunnett's multiple comparisons test following repeated measures one-
896 way ANOVA, $p = 0.00922$) and PPRs (filled bars; $p = 0.512$, repeated measures one-way
897 ANOVA, $p = 0.00922$).
898 D, same as B, but with a higher concentration of forskolin (100 μM; $n = 6$). Horizontal and
899 vertical scale bars indicate 300 ms and 50 pA, respectively.
900 E, quantification of the data shown in D. 1-min injection of a high concentration of forskolin
901 alone did not induce consistent changes in first EPSC amplitudes ($p = 0.0886$, repeated measures
902 one-way ANOVA) and PPRs ($p = 0.0370$ and 0.419 from left to right, Dunnett's multiple
903 comparisons test following repeated measures one-way ANOVA, $p = 0.00796$).
904 F, same as B, but 1-min forskolin (10 μM) injection was paired with α/β KC activation ($n = 5$).
905 Horizontal and vertical scale bars indicate 300 ms and 100 pA, respectively.

906 G, quantification of the data shown in F. 1-min pairing of a low concentration of forskolin and
907 α/β KC activation induced coherent but transient depression in first EPSC amplitudes and
908 facilitation of PPRs. P values for EPSCs are (from left to right) $< 10^{-5}$, 0.0105 and 0.0505
909 (Dunnett's multiple comparisons test following repeated measures one-way ANOVA, $p < 10^{-4}$)
910 and for PPRs, 0.0117, 0.415 and 0.187 (repeated measures one-way ANOVA, $p < 10^{-3}$).
911 H, same as F, but with a higher concentration of forskolin (100 μM; n =5). Horizontal and
912 vertical scale bars indicate 300 ms and 50 pA, respectively.
913 I, quantification of the data shown in H. 1-min pairing of a high concentration of forskolin and
914 α/β KC activation induced coherent but transient depression in first EPSC amplitudes and
915 facilitation of PPRs. P values for EPSCs are (from left to right) $< 10^{-3}$, 0.208 and 0.997
916 (Dunnett's multiple comparisons test following repeated measures one-way ANOVA, $p < 10^{-3}$)
917 and for PPRs, 0.00258, 0.998 and 0.206 (repeated measures one-way ANOVA, $p < 10^{-3}$).
918 J, same as B, but instead of forskolin, only the solvent DMSO (0.1 %) was injected (n = 4). 1-
919 min injection was repeated 3 times with 1-min intervals so that the data could also serve as
920 control for the experiments shown in Fig. 8. Horizontal and vertical scale bars indicate 300 ms
921 and 100 pA, respectively.
922 K, quantification of the data shown in J. DMSO injection alone did not affect first EPSC
923 amplitudes (p = 0.272, repeated measures one-way ANOVA) or PPRs (p = 0.108).

924 **Figure 8. Simultaneous activation of cGMP pathway and α/β KCs induces presynaptic LTP**

925 A, a schematic of the experiments. BAY 41-2272 was focally applied to the dendritic region of
926 the MBON-γ1pedc via an injection pipette while measuring optogenetically evoked α/β KC-to-
927 MBON-γ1pedc EPSCs.
928 B, first EPSC amplitudes (open circles, mean ± s.e.m; n = 4) and PPRs (filled circles) plotted
929 against time after the end of the three repeats of 1-min injection of BAY 41-2272 (100 μM). The
930 data were normalized to the average of a 3-min baseline recorded before pairing. Upper right
931 traces show overlaid representative EPSCs sampled before (at −6 min; black) and after (at 17
932 min; red) injection. Horizontal and vertical scale bars in this and the other panels indicate 300 ms
933 and 100 pA, respectively. Lower right traces show the same EPSCs normalized with the first
934 EPSC amplitude.
935 C, quantification of the data shown in B at early, middle and late periods after injection (mean ±

936 s.e.m.). Black dots indicate data from individual cells. BAY 41-2272 injection alone a delayed
937 potentiation of first EPSC amplitudes (open bars) without coherent changes in PPRs (filled bars).
938 P values for EPSCs are (from left to right), 0.631, 0.00915 and 0.00302 (Dunnett's multiple
939 comparisons test following repeated measures one-way ANOVA, $p = 0.00307$), and for PPRs,
940 0.383, 0.760 and 0.261 (repeated measures one-way ANOVA, $p = 0.0579$).
941 D, same as B, but BAY 41-2272 injection was paired with α/β KC activation ($n = 5$).
942 E, quantification of the data shown in D. pairing of BAY 41-2272 and α/β KC activation
943 potentiated first EPSC amplitudes and decreased PPRs at the later time points. P values for
944 EPSCs are (from left to right) 0.488, 0.0605, and 0.0360 (Dunnett's multiple comparisons test
945 following repeated measures one-way ANOVA, $p = 0.0502$), and for PPRs, $< 10^{-5}$, $< 10^{-5}$ and $<$
946 10^{-6} (repeated measures one-way ANOVA, $p < 10^{-6}$).

947 **Figure S1. Transcriptome data related to pharmacological target molecules**

948 Cell-type-specific transcriptome data of the genes encoding the target molecules of
949 pharmacology used in this work. This figure was recreated based on published data (Aso *et al.*,
950 2019). PPL-γ1pedc is the DAN whose axonal innervation pattern in the MB lobes matches the
951 dendritic arborization of MBON-γ1pedc.

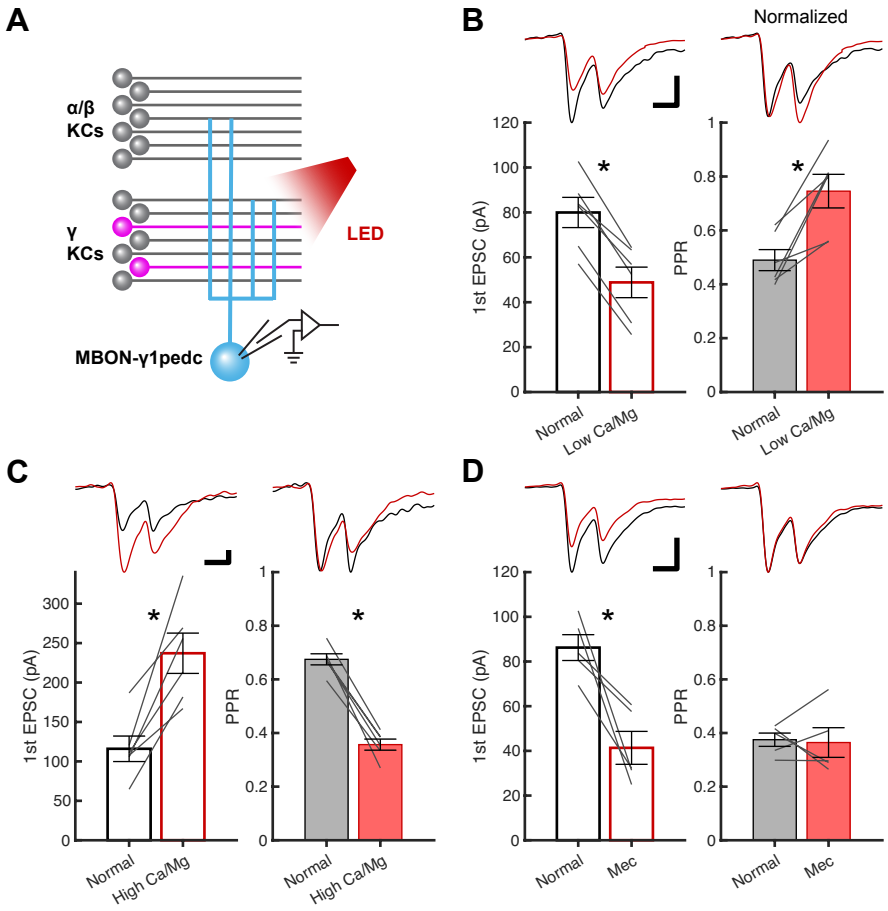
A
α/β
KCs
γ
KCs
LED
MBON-γ1pedc
B
Normalized
1st EPSC (pA)
PPR
Normal
Low Ca/Mg
C
1st EPSC (pA)
PPR
Normal
High Ca/Mg
D
1st EPSC (pA)
PPR
Normal
Mec

Figure 1

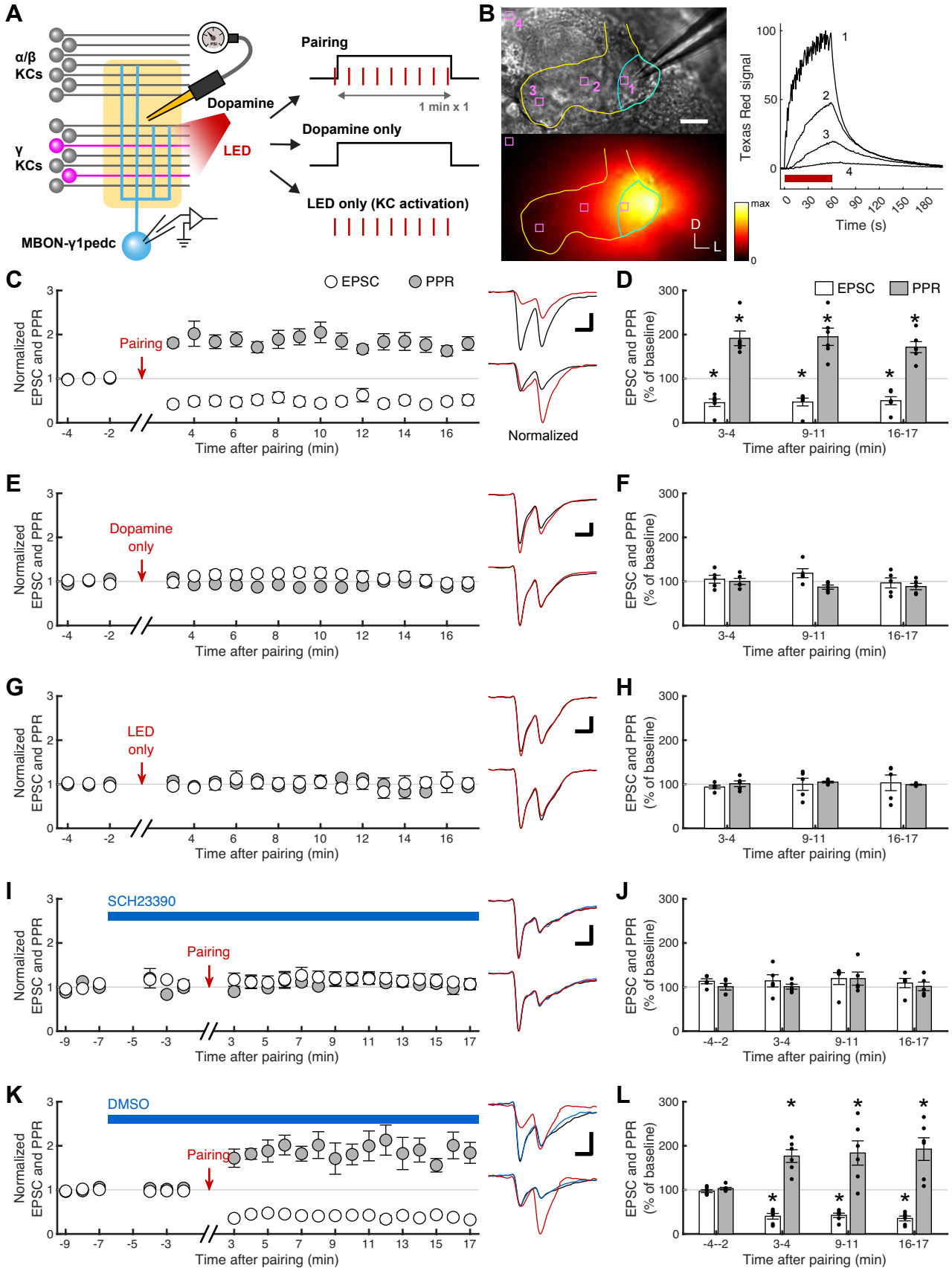
A
α/β KCs
γ KCs
Dopamine
LED
MBON-γ1pedc
Pairing
1 min x 1
Dopamine only
LED only (KC activation)
B
Texas Red signal
Time (s)
max
D
L
C
EPSC
PPR
Normalized EPSC and PPR
Pairing
Time after pairing (min)
Normalized
D
EPSC and PPR (% of baseline)
3-4
9-11
16-17
E
Dopamine only
F
G
LED only
H
I
SCH23390
J
-4--2
K
DMSO
L

Figure 2

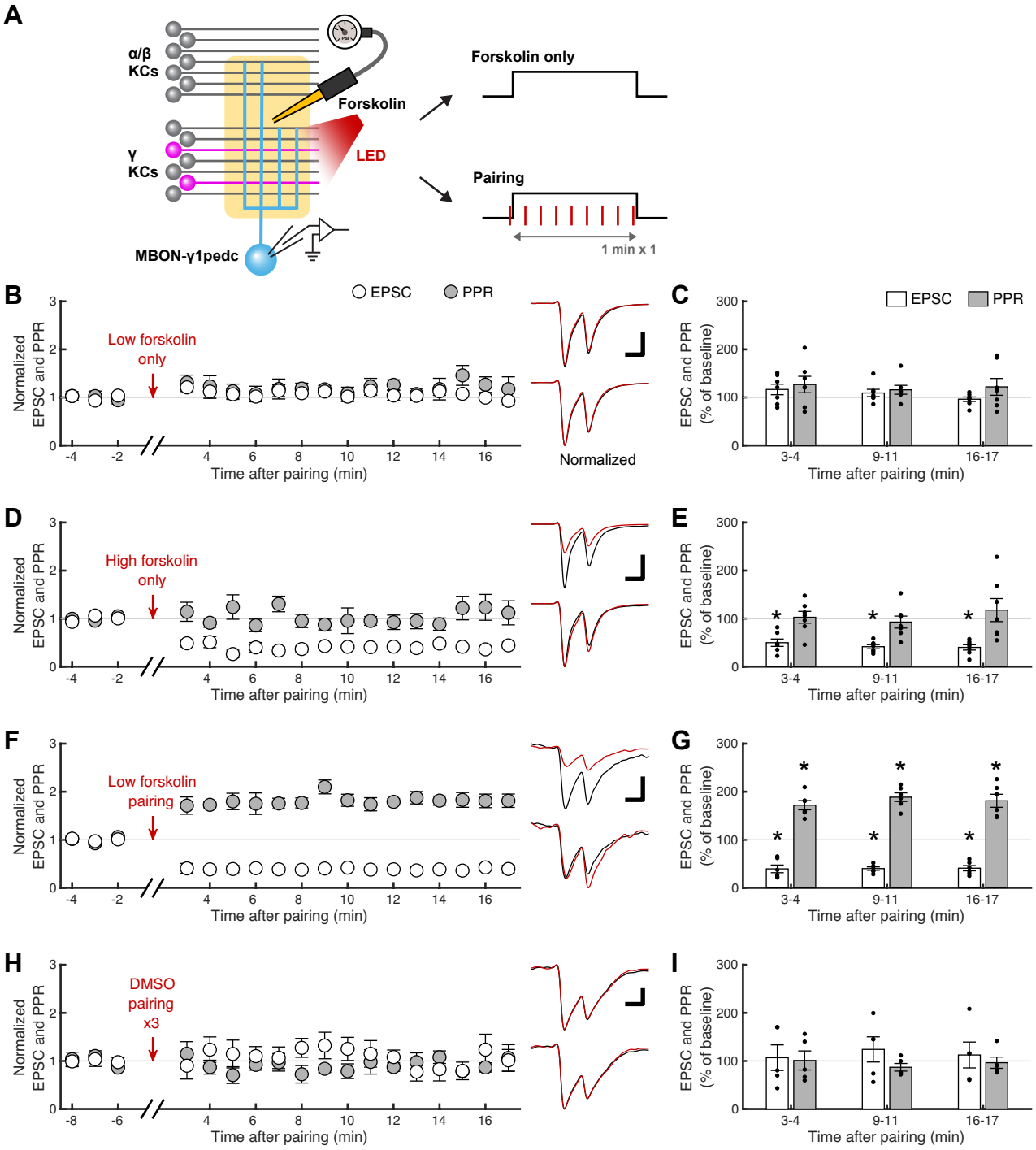
A
α/β KCs
γ KCs
Forskolin
LED
MBON-γ1pedc
Forskolin only
Pairing
1 min x 1
B
EPSC
PPR
Low forskolin only
Normalized EPSC and PPR
Time after pairing (min)
Normalized
C
EPSC
PPR
EPSC and PPR (% of baseline)
3-4
9-11
16-17
Time after pairing (min)
D
High forskolin only
E
F
Low forskolin pairing
G
H
DMSO pairing x3
I

Figure 3

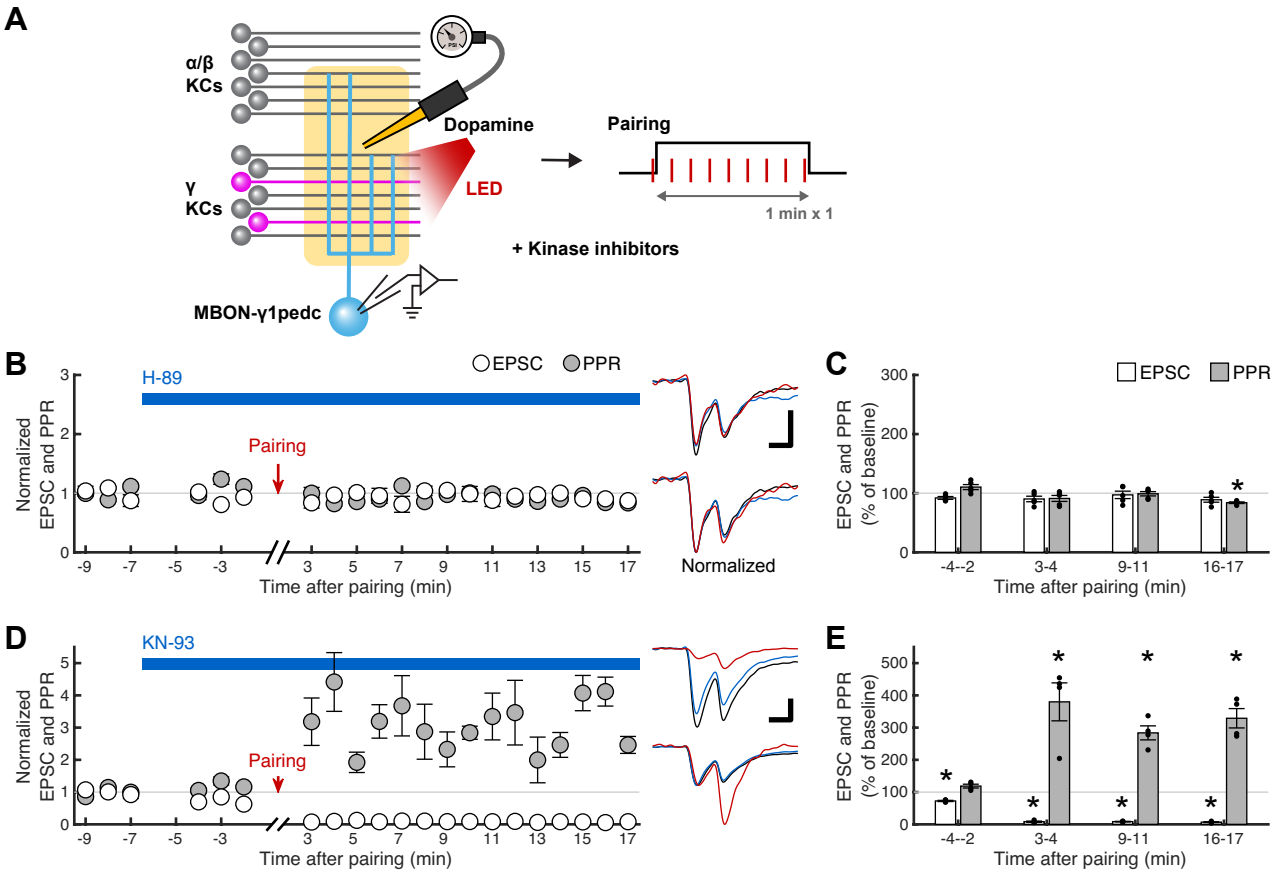
A
α/β KCs
γ KCs
Dopamine
LED
MBON-γ1pedc
Pairing
1 min x 1
+ Kinase inhibitors
B
H-89
EPSC
PPR
Pairing
Normalized EPSC and PPR
Time after pairing (min)
Normalized
C
EPSC
PPR
EPSC and PPR (% of baseline)
-4--2
3-4
9-11
16-17
Time after pairing (min)
D
KN-93
Pairing
Normalized EPSC and PPR
Time after pairing (min)
E
EPSC and PPR (% of baseline)
-4--2
3-4
9-11
16-17
Time after pairing (min)

Figure 4

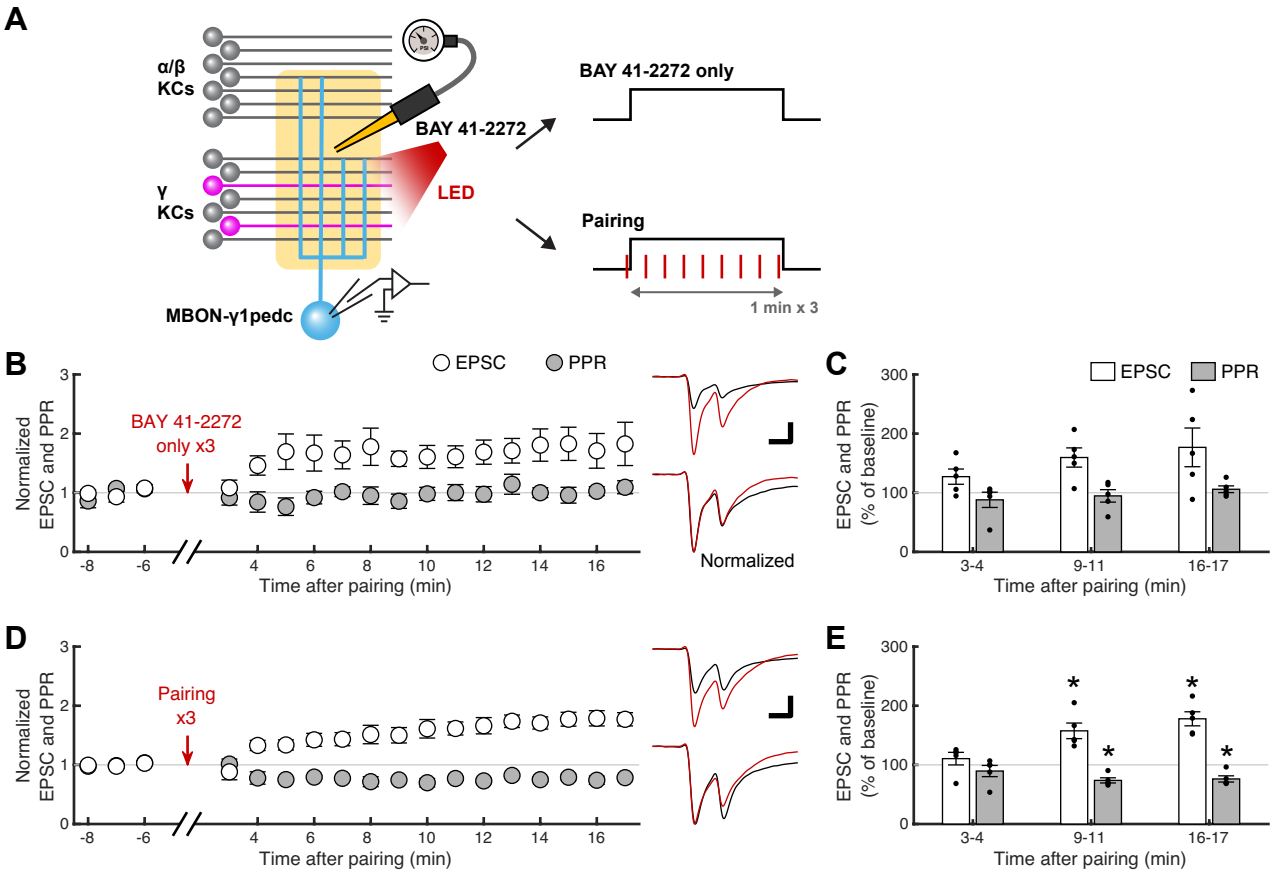
A
α/β KCs
γ KCs
BAY 41-2272
LED
MBON-γ1pedc
BAY 41-2272 only
Pairing
1 min x 3
B
EPSC
PPR
Normalized EPSC and PPR
BAY 41-2272 only x3
Time after pairing (min)
Normalized
C
EPSC
PPR
EPSC and PPR (% of baseline)
3-4
9-11
16-17
Time after pairing (min)
D
Normalized EPSC and PPR
Pairing x3
Time after pairing (min)
E
EPSC and PPR (% of baseline)
3-4
9-11
16-17
Time after pairing (min)

Figure 5

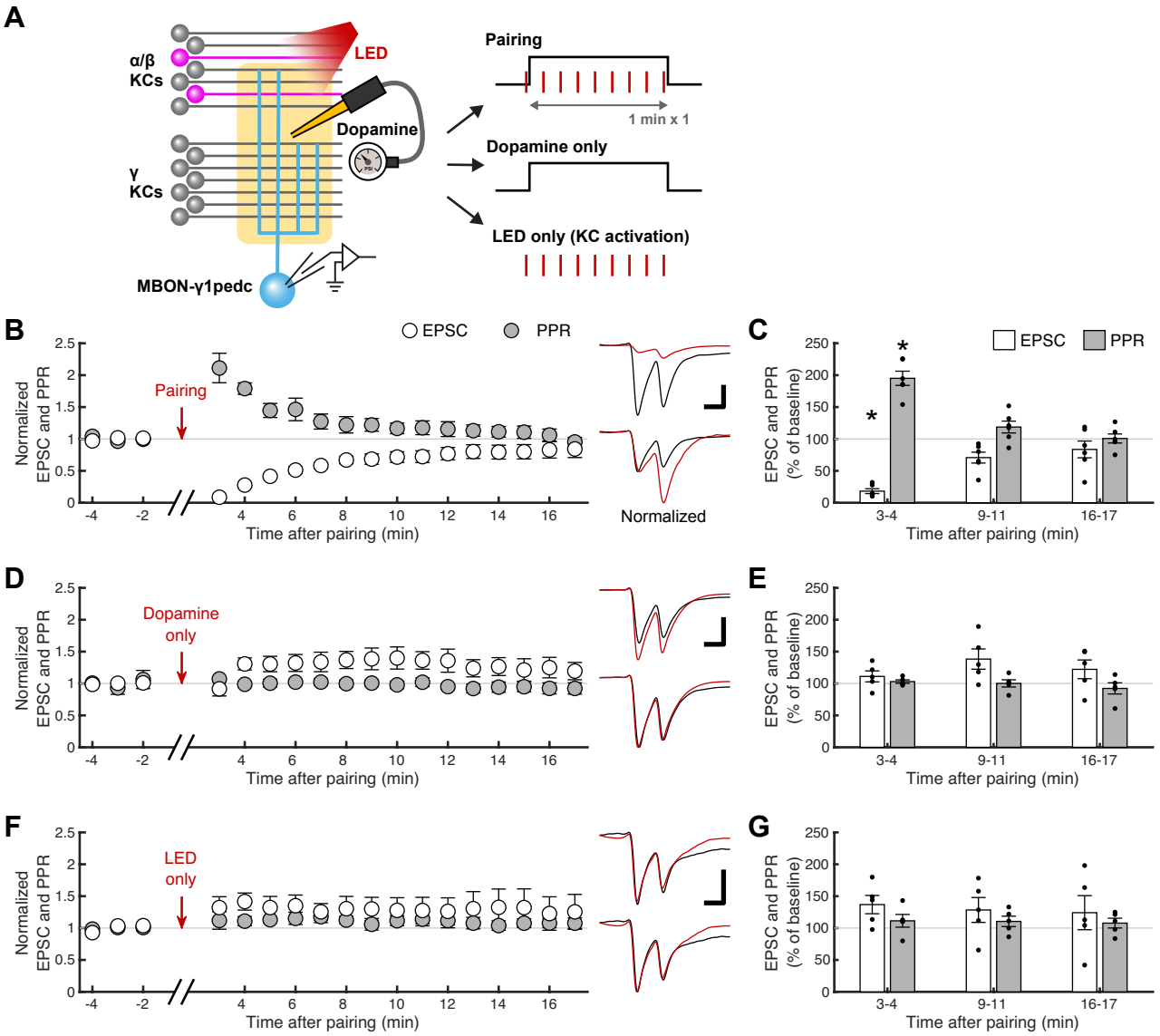
A
α/β KCs
γ KCs
LED
Dopamine
MBON-γ1pedc
Pairing
1 min x 1
Dopamine only
LED only (KC activation)
B
EPSC
PPR
Pairing
Normalized EPSC and PPR
Time after pairing (min)
Normalized
C
EPSC
PPR
EPSC and PPR (% of baseline)
3-4
9-11
16-17
Time after pairing (min)
D
Dopamine only
E
F
LED only
G

Figure 6

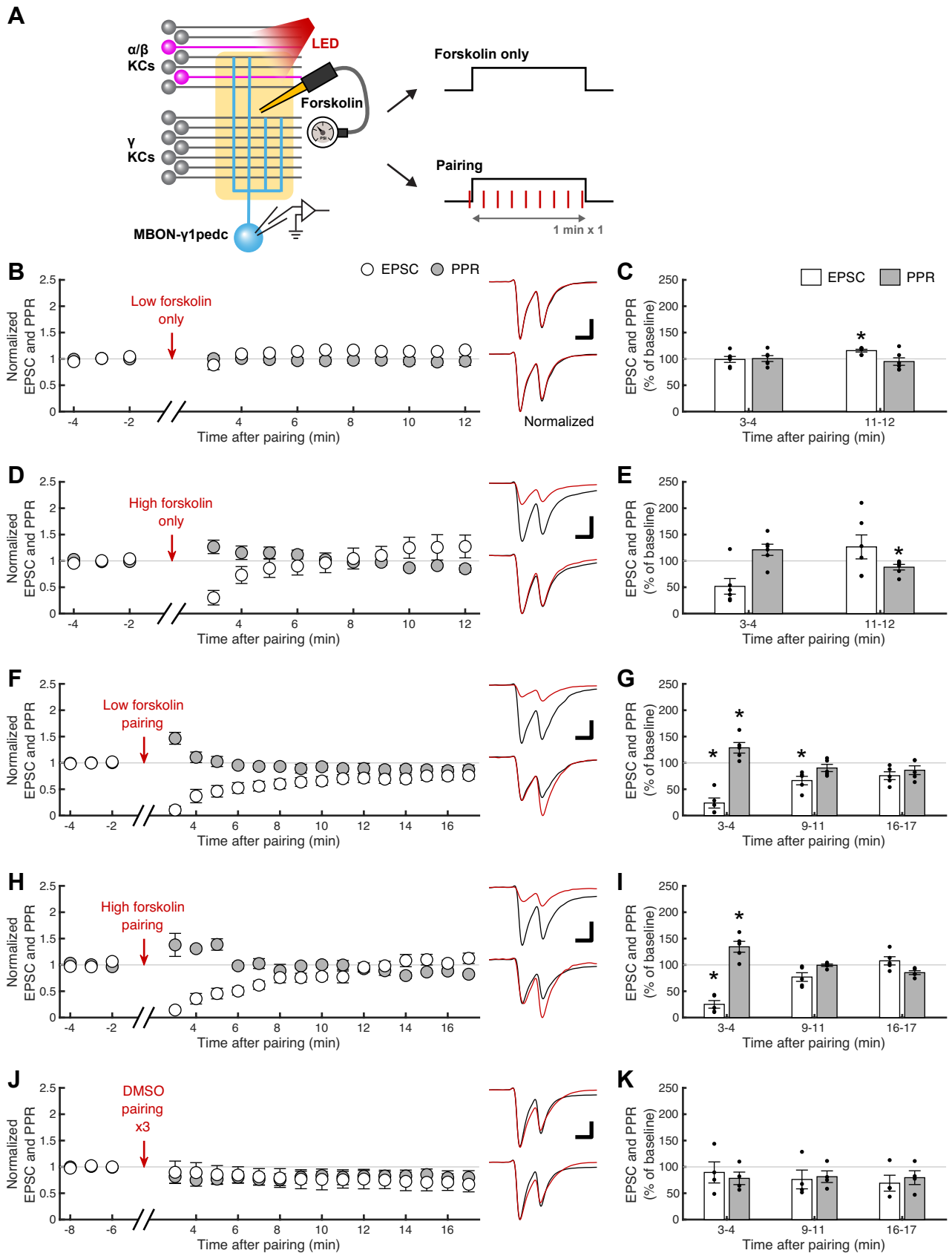
A
α/β KCs
γ KCs
LED
Forskolin
MBON-γ1pedc
Forskolin only
Pairing
1 min x 1
B
EPSC
PPR
Low forskolin only
Normalized EPSC and PPR
Time after pairing (min)
Normalized
C
EPSC and PPR (% of baseline)
3-4
11-12
D
High forskolin only
E
F
Low forskolin pairing
G
9-11
16-17
H
High forskolin pairing
I
J
DMSO pairing x3
K

Figure 7

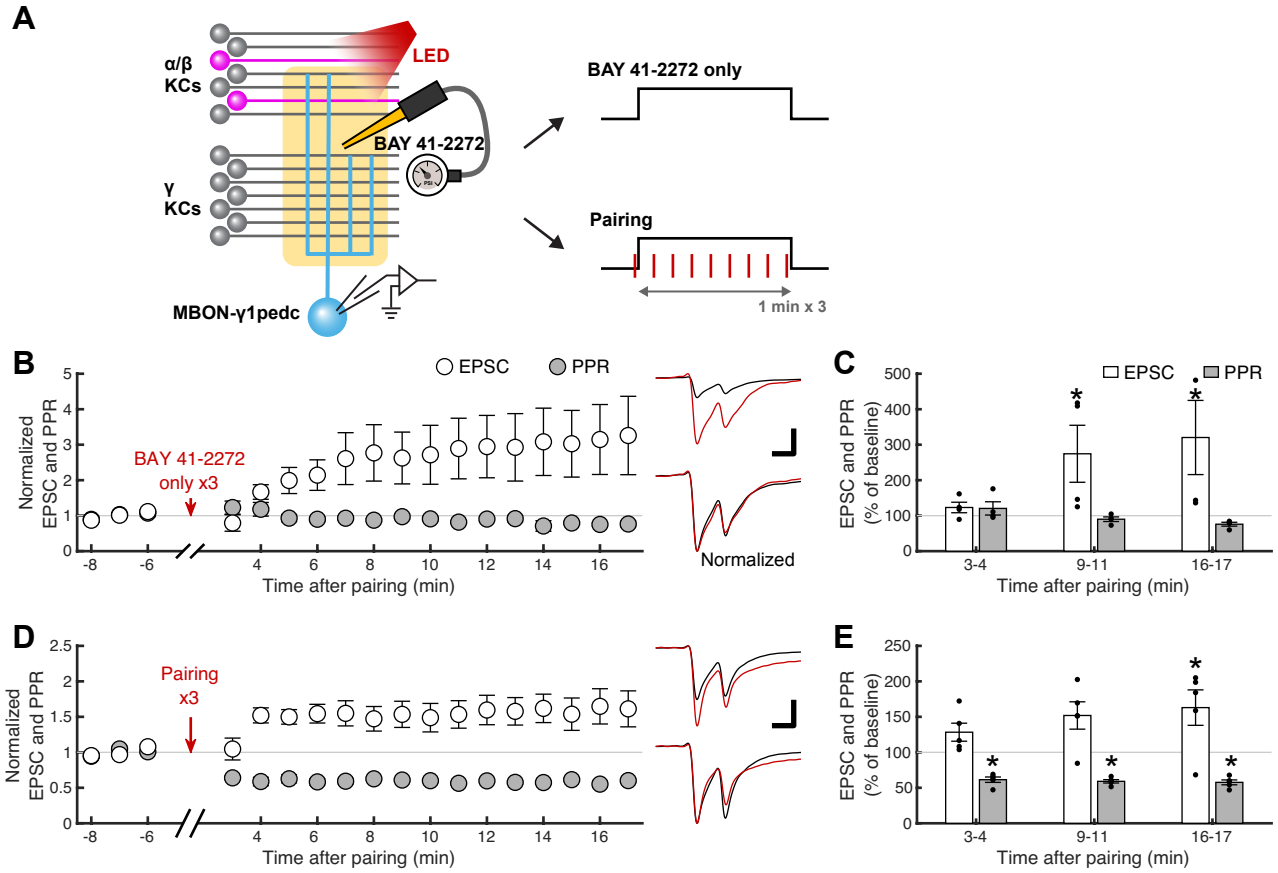
A
α/β KCs
γ KCs
LED
BAY 41-2272
MBON-γ1pedc
BAY 41-2272 only
Pairing
1 min x 3
B
EPSC
PPR
Normalized EPSC and PPR
BAY 41-2272 only x3
Time after pairing (min)
Normalized
C
EPSC
PPR
EPSC and PPR (% of baseline)
3-4
9-11
16-17
Time after pairing (min)
D
Normalized EPSC and PPR
Pairing x3
Time after pairing (min)
E
EPSC and PPR (% of baseline)
3-4
9-11
16-17
Time after pairing (min)

Figure 8

Full name	FlyBase ID	Symbol	γ KC	α/β KC	MBON-γ1pedc	PPL1-γ1pedc
rutabaga	FBtr0073992	rut-RA	378	349	4	3
rutabaga	FBtr0305581	rut-RB	0	0	2	12
rutabaga	FBtr0333654	rut-RC	13	7	1	0
rutabaga	FBtr0333655	rut-RD	7	6	2	2
rutabaga	FBtr0333656	rut-RE	0	0	2	11
rutabaga	FBtr0333657	rut-RF	301	135	2	1
rutabaga	FBtr0340467	rut-RG	0	0	1	0
Adenylyl cyclase 13E	FBtr0074073	Ac13E-RA	1	1	0	0
Adenylyl cyclase 13E	FBtr0100142	Ac13E-RB	0	0	1	1
Adenylyl cyclase 13E	FBtr0332497	Ac13E-RC	2	0	9	5
Adenylyl cyclase 76E	FBtr0074897	Ac76E-RA	10	3	2	20
Adenylyl cyclase 76E	FBtr0304746	Ac76E-RB	9	0	6	1
Adenylyl cyclase 78C	FBtr0301701	Ac78C-RB	14	1	1	0
Adenylyl cyclase 78C	FBtr0305501	Ac78C-RC	0	0	0	3
Adenylyl cyclase 78C	FBtr0330066	Ac78C-RD	12	2	1	0
Adenylyl cyclase 78C	FBtr0330067	Ac78C-RE	14	1	1	0
Adenylyl cyclase 78C	FBtr0333358	Ac78C-RF	10	0	0	1
Adenylyl cyclase X A	FBtr0080415	ACXA-RA	0	0	0	0
Adenylyl cyclase X A	FBtr0305490	ACXA-RC	0	0	0	0
Adenylyl cyclase X A	FBtr0305491	ACXA-RD	0	0	0	0
Adenylyl cyclase X A	FBtr0333225	ACXA-RG	0	0	0	0
Adenylyl cyclase X A	FBtr0344132	ACXA-RH	0	0	0	0
Adenylyl cyclase X B	FBtr0080414	ACXB-RA	0	0	0	0
Adenylyl cyclase X C	FBtr0080413	ACXC-RA	0	1	0	0
Adenylyl cyclase X C	FBtr0100494	ACXC-RB	0	0	0	0
Adenylyl cyclase X D	FBtr0072874	ACXD-RA	0	0	0	0
Adenylyl cyclase X D	FBtr0332662	ACXD-RB	0	0	0	0
Adenylyl cyclase X E	FBtr0310556	ACXE-RB	0	0	0	0
Protein kinase, cAMP-dependent, catalytic subunit 1	FBtr0079851	Pka-C1-RB	1739	945	69	378
Protein kinase, cAMP-dependent, catalytic subunit 1	FBtr0079852	Pka-C1-RC	194	204	6	41
Protein kinase, cAMP-dependent, catalytic subunit 1	FBtr0335495	Pka-C1-RD	147	170	31	19
Protein kinase, cAMP-dependent, catalytic subunit 2	FBtr0085727	Pka-C2-RB	0	0	0	0
Protein kinase, cAMP-dependent, catalytic subunit 2	FBtr0335454	Pka-C2-RC	0	0	0	0
Protein kinase, cAMP-dependent, catalytic subunit 3	FBtr0075529	Pka-C3-RA	221	1	7	8
Protein kinase, cAMP-dependent, catalytic subunit 3	FBtr0075528	Pka-C3-RB	0	0	0	0
Protein kinase, cAMP-dependent, regulatory subunit type 1	FBtr0302641	Pka-R1-RAA	0	53	6	0
Protein kinase, cAMP-dependent, regulatory subunit type 1	FBtr0302642	Pka-R1-RAB	0	30	0	0
Protein kinase, cAMP-dependent, regulatory subunit type 1	FBtr0302643	Pka-R1-RAC	77	24	1	11
Protein kinase, cAMP-dependent, regulatory subunit type 1	FBtr0299891	Pka-R1-RK	204	142	20	42
Protein kinase, cAMP-dependent, regulatory subunit type 1	FBtr0299892	Pka-R1-RL	0	0	0	0
Protein kinase, cAMP-dependent, regulatory subunit type 1	FBtr0300528	Pka-R1-RM	0	0	0	0
Protein kinase, cAMP-dependent, regulatory subunit type 1	FBtr0300529	Pka-R1-RN	0	0	0	0
Protein kinase, cAMP-dependent, regulatory subunit type 1	FBtr0299893	Pka-R1-RO	0	36	3	2
Protein kinase, cAMP-dependent, regulatory subunit type 1	FBtr0300530	Pka-R1-RP	0	0	0	0
Protein kinase, cAMP-dependent, regulatory subunit type 1	FBtr0300531	Pka-R1-RQ	0	0	0	0
Protein kinase, cAMP-dependent, regulatory subunit type 1	FBtr0300532	Pka-R1-RR	0	0	0	0
Protein kinase, cAMP-dependent, regulatory subunit type 1	FBtr0300533	Pka-R1-RS	173	7	1	41
Protein kinase, cAMP-dependent, regulatory subunit type 1	FBtr0300534	Pka-R1-RT	0	0	0	0
Protein kinase, cAMP-dependent, regulatory subunit type 1	FBtr0300535	Pka-R1-RU	0	0	0	0
Protein kinase, cAMP-dependent, regulatory subunit type 1	FBtr0302637	Pka-R1-RV	143	76	7	4
Protein kinase, cAMP-dependent, regulatory subunit type 1	FBtr0302638	Pka-R1-RW	26	35	12	14
Protein kinase, cAMP-dependent, regulatory subunit type 1	FBtr0302639	Pka-R1-RX	148	76	7	88
Protein kinase, cAMP-dependent, regulatory subunit type 1	FBtr0302640	Pka-R1-RZ	319	44	15	9
Protein kinase, cAMP-dependent, regulatory subunit type 2	FBtr0088437	Pka-R2-RA	28	79	14	7
Protein kinase, cAMP-dependent, regulatory subunit type 2	FBtr0088438	Pka-R2-RB	2086	1248	63	274
Protein kinase, cAMP-dependent, regulatory subunit type 2	FBtr0112901	Pka-R2-RD	0	0	0	0
Protein kinase, cAMP-dependent, regulatory subunit type 2	FBtr0112902	Pka-R2-RE	23	35	5	6
Calcium/calmodulin-dependent protein kinase II	FBtr0089218	CaMKII-RA	203	138	2	157
Calcium/calmodulin-dependent protein kinase II	FBtr0089219	CaMKII-RB	0	1	0	0
Calcium/calmodulin-dependent protein kinase II	FBtr0089217	CaMKII-RC	0	0	0	0
Calcium/calmodulin-dependent protein kinase II	FBtr0100146	CaMKII-RD	71	56	23	70
Calcium/calmodulin-dependent protein kinase II	FBtr0100147	CaMKII-RE	39	47	19	69
Calcium/calmodulin-dependent protein kinase II	FBtr0100148	CaMKII-RG	16	15	2	14
Calcium/calmodulin-dependent protein kinase II	FBtr0300377	CaMKII-RH	40	38	20	23
Calcium/calmodulin-dependent protein kinase II	FBtr0300378	CaMKII-RI	15	14	0	12
Calcium/calmodulin-dependent protein kinase II	FBtr0300379	CaMKII-RJ	31	23	13	19
Calcium/calmodulin-dependent protein kinase II	FBtr0333673	CaMKII-RK	11	11	0	6
Calcium/calmodulin-dependent protein kinase II	FBtr0333674	CaMKII-RL	7	26	4	4
Calcium/calmodulin-dependent protein kinase II	FBtr0333675	CaMKII-RM	12	11	1	1
Guanylyl cyclase α-subunit at 99B	FBtr0085453	Gycα99B-RA	98	67	22	16
Guanylyl cyclase β-subunit at 100B	FBtr0085753	Gycβ100B-RA	42	38	7	18
Dopamine 1-like receptor 1	FBtr0290283	Dop1R1-RB	0	13	0	0
Dopamine 1-like receptor 1	FBtr0301351	Dop1R1-RC	148	85	1	0
Dopamine 1-like receptor 1	FBtr0308191	Dop1R1-RD	524	244	24	20
Dopamine 1-like receptor 1	FBtr0330711	Dop1R1-RE	0	13	0	0
Dopamine 1-like receptor 1	FBtr0346763	Dop1R1-RF	0	13	0	0
Dopamine 1-like receptor 2	FBtr0085467	Dop1R2-RA	22	11	1	1
Dopamine 1-like receptor 2	FBtr0085468	Dop1R2-RB	117	121	1	0
Dopamine 1-like receptor 2	FBtr0330293	Dop1R2-RC	22	11	1	1

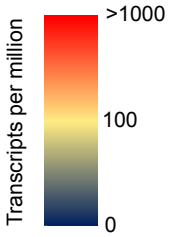

Figure S1